

1 **Strong dependence of wintertime Arctic moisture and cloud distributions on atmospheric**
2 **large-scale circulation**

3 Tiina Nygård^{1*}, Rune G. Graversen², Petteri Uotila³, Tuomas Naakka¹, Timo Vihma¹

4 ¹Finnish Meteorological Institute, Helsinki, Finland, ²Department of Physics and Technology,
5 University of Tromsø, Tromsø, Norway, ³Institute for Atmospheric and Earth System Research
6 (INAR)/Physics, University of Helsinki, Helsinki, Finland

7 * Corresponding author (email: tiina.nygard@fmi.fi)

8 **ABSTRACT**

9 This study gives a comprehensive picture on how atmospheric large-scale circulation is related to
10 moisture transport, and to distributions of moisture, clouds and surface downward longwave
11 radiation in the Arctic in winter. Anomaly distributions of above-mentioned variables are
12 compared in 30 characteristic wintertime atmospheric circulation regimes, which are allocated
13 from 15 years (2003–2017) of mean sea-level pressure (MSLP) data of ERA-Interim reanalysis
14 applying the Self-Organizing Map (SOM) method. The characteristic circulation regimes are
15 further related to known climate indices: the North Atlantic Oscillation (NAO), the Arctic
16 Oscillation (AO), and Greenland Blocking Index (GBI), as well as to a frequent high-pressure
17 pattern across the Arctic Ocean from Siberia to North America, called here as the Arctic Bridge.
18 Effects of large-scale circulation on moisture, cloud and longwave radiation are to a large extent
19 occurring through the impact of horizontal moisture transport. Evaporation is typically not
20 efficient enough to shape those distributions, and much of the moisture evaporated in the Arctic
21 is transported southwards. The positive phase of the NAO and AO increases moisture and clouds
22 in the Northern Europe and eastern North Atlantic, and a strong Greenland blocking typically
23 increases those in the southwest of Greenland. When the Arctic Bridge is lacking, the amount of
24 moisture, clouds and downward longwave radiation is anomalously high near the North Pole. Our
25 results reveal a strong dependence of moisture, clouds and longwave radiation on atmospheric
26 pressure fields, which also appears important in a climate change perspective.

27

28 **1. Introduction**

29 Atmospheric moisture and clouds play a central role in radiative processes (Morrison et al. 2011)
30 and the hydrological cycle (Vihma et al. 2016) in the Arctic. Through radiation, clouds and
31 atmospheric moisture regulate the surface energy balance and surface temperature. For most of
32 the year, including winter, clouds have a warming impact on the surface because they reduce the
33 surface energy loss by re-emitting longwave radiation back to the surface (Shupe and Intrieri
34 2004). The phase of the cloud condensate has a large impact on the radiative processes as liquid
35 water in clouds more efficiently absorbs and re-emits longwave radiation compared to frozen
36 water (Shupe and Intrieri 2004). In winter, the air temperature is typically well below the freezing
37 point and temperature changes do not often cause surface melt, but higher temperatures can
38 reduce sea ice growth, resulting in thinner sea ice, which is also more vulnerable to melt in the
39 following spring and summer (Screen and Simmonds 2010; Stroeve and Notz 2018).

40 The dramatic warming of the Arctic, known as Arctic Amplification, and the sea ice concentration
41 decline observed during the recent decades have been attributed to several feedback processes,
42 such as lapse-rate, surface albedo and Planck feedbacks, but also to changes in large-scale
43 circulation, atmospheric moisture transport and clouds (Graversen and Wang 2009; Doyle et al.
44 2011; Liu et al. 2012; Pithan and Mauritsen 2014; Park et al. 2015; Woods and Caballero 2016;
45 Gong et al. 2017; Johansson et al. 2017; Gimeno-Sotelo et al. 2018; Pithan et al. 2018). Park et
46 al. (2015) addressed causality of processes related to clouds and radiation based on 33 winters
47 of ERA-Interim reanalysis data and satellite data. They showed based on lead/lag time analyses
48 that a positive anomaly in horizontal moisture transport and warm air advection typically

49 initializes an increase in the vertically integrated total column water and suppresses evaporation.
50 Shortly afterwards, an increase in downward longwave radiation follows, which affects sea ice.
51 These findings were supported by Gong et al. (2017). Furthermore, reduced sea ice concentration
52 in winter has been found to correlate in many locations with increased surface evaporation and
53 upward latent heat flux (Screen and Simmonds 2010; Jun et al. 2016), and has led to locally
54 increased cloud formation and enhancement in longwave radiation towards the surface (Jun et
55 al. 2016). This has strengthened the cloud-temperature-moisture relationship in the lower
56 troposphere during the last decades (Morrison et al. 2019). Based on the above mentioned
57 studies, it can be inferred that the sea ice–cloud interactions are presumably acting in two
58 directions and causing a positive feedback loop in winter: an increased cloud cover may reduce
59 sea ice concentration which in turn may further increase cloud cover.

60 The importance of moisture transport for the cloud cover in the Arctic was already recognized by
61 Curry and Herman (1985), who linked synoptic situation, moisture transport and cloud cover, and
62 found the large-scale moisture transport to be important in the Beaufort Sea region, especially
63 for middle-level cloud cover. In addition, Walsh and Chapman (1998) demonstrated a
64 relationship between sea-level pressure and cloud cover in the central Arctic. Moisture transport
65 to the Arctic, cloud cover and cloud water content have also been shown to be associated with
66 the variations of the Arctic Oscillation (AO) (Eastman and Warren 2010; Devasthale et al. 2012;
67 Jun et al. 2016). Recently, much research focus has been on moisture intrusions, which are
68 narrow plumes of anomalously warm and moist air, typically accompanied by increased cloud
69 amount and enhanced downward longwave radiation (Woods et al. 2013; Johansson et al. 2017;
70 Liu et al. 2018), penetrating to the Arctic. The intrusions are responsible for a major part of the

71 moisture transport to the Arctic, and they are found to be associated to a dipole-like large-scale
72 flow pattern with a blocking high to the east and a low pressure to the west (Skific et al. 2009;
73 Woods et al. 2013; Liu and Barnes 2015). This dipole-like pattern enables a more meridional
74 flow from mid latitudes to access the Arctic Ocean. Pithan et al. (2018) pointed out that notable
75 air-mass transformations take place along the path of intrusions, and in particular, phase changes
76 from liquid water to frozen water are critical for the radiative effects of clouds and for cloud
77 decay and dissipation. Most of the moisture transported to the Arctic has its origin in the Atlantic
78 Ocean and the Pacific Ocean, especially in winter (Vázquez et al. 2016; Zhong et al. 2018), and
79 the local moisture flux from the surface (i.e., evaporation) in the Arctic is estimated to provide
80 only about 10 % of the total column water vapor on a yearly basis (Boisvert et al. 2015).

81 Despite the inevitable importance of atmospheric moisture and clouds on the Arctic climate, their
82 distributions, properties and climate impacts are still poorly known, especially in winter. Previous
83 studies, cited above, have contributed to understanding of the climatology of moisture and
84 clouds in the Arctic, feedback processes related to moisture and clouds, intensive moisture
85 intrusions, and, very recently, also the impacts of intensive moisture intrusions on clouds.
86 However, most studies have been restricted to intensive events, certain circulation types, or
87 patterns associated with the North Atlantic Oscillation (NAO) and AO only (Devasthale et al.
88 2012; Woods et al. 2013; Liu et al. 2018). This study intends to expand our knowledge on those
89 topics by offering, for the first time, a systematic picture on how atmospheric large-scale
90 circulation is related to moisture transport, distributions of moisture and clouds, and surface
91 downward longwave radiation in wintertime in the current climate of the circumpolar Arctic. This
92 is done by applying the Self-Organizing Map (SOM) method (Kohonen 2001) which enables a

93 comprehensive analysis of a large variety of atmospheric circulation regimes. In this study,
94 anomaly distributions of atmospheric moisture transport, moisture, clouds and downward
95 longwave radiation are related to 30 characteristic wintertime atmospheric circulation regimes,
96 which are allocated from 15 years (2003–2017) of mean sea-level pressure (MSLP) data applying
97 the SOM method. The data are taken from an atmospheric reanalysis, ERA-Interim (Dee et al.
98 2011) of the European Centre for Medium-Range Weather Forecasts (ECMWF), which assimilates
99 the existing observations into a numerical weather prediction model thereby offering a gridded
100 and coherent representation of circulation patterns, moisture and clouds. We also give insights
101 into regional and vertical distributions of the moisture and cloud variables in different circulation
102 regimes. Furthermore, we demonstrate and discuss connections of moisture and cloud
103 distributions and their anomalies to known climate indices, such as the NAO and AO, as well as
104 to some other frequently occurring atmospheric circulation patterns. The results of this study
105 provide a solid basis for further studies addressing changes and trends in atmospheric circulation
106 and their influence on moisture and clouds in the Arctic.

107 **2. Data and methods**

108 **a. ERA-Interim**

109 In this study, gridded fields of mean sea-level pressure, wind components, moisture and cloud
110 variables as well as downward longwave radiation at the surface were analysed for winters
111 (December to February, DJF) during the period 2003–2017 in the circumpolar Arctic north of
112 55°N. This 15-year-long study period represents “the new climate” of the Arctic, with decreased
113 sea ice concentration, increased surface temperature and cloud cover (Jun et al. 2016). The

114 analyses were based on ERA-Interim (Dee et al. 2011). ERA-Interim represents a state-of-the-art
115 global atmospheric reanalysis. It applies a four-dimensional variational data assimilation method
116 to assimilate a variety of observations, including, e.g., radiosonde observations, satellite
117 radiances, and infrared spectrometer observations from the Atmospheric Infrared Sounder
118 (AIRS). The spectral model resolution of ERA-interim is T255, and the data utilized in this study
119 have a horizontal resolution of $0.75^\circ \times 0.75^\circ$. ERA-Interim has 60 vertical model levels, but, for
120 simplicity, we only show results based on pressure level data (except for vertically integrated
121 products of ERA-Interim calculated directly on model levels). The pressure level data are provided
122 at a 25-hPa vertical interval from 1000 hPa to 750 hPa and at a 50-hPa interval from 750 hPa to
123 300 hPa. Our comparison of results based on model-level and pressure-level data supported this
124 choice: results for horizontal moisture transport based on model-level data, with the mass
125 correction method of Trenberth (1991) applied to correct erroneous mass fluxes associated with
126 spurious winds, were practically the same as the results based on pressure-level data. This small
127 difference between model- and pressure level data has also been noticed by Dufour et al. (2016).
128 The reanalysis output was analysed at 6-hour intervals. Most of the variables are available at 6-
129 hour intervals in the reanalysis, but evaporation, divergence of horizontal moisture transport and
130 downward longwave radiation are not analysis variables and were taken from 6- and 12-hour
131 forecasts.

132 Whereas atmospheric humidity is assimilated in ERA-Interim, clouds are entirely modelled
133 entities which are only indirectly constrained by assimilation of observations. The cloud
134 parameterization scheme of ERA-Interim is based on the approach of Tiedtke (1993). ERA-Interim
135 has two prognostic cloud variables: cloud fraction and cloud condensate. Partitioning of cloud

136 condensate to liquid water and frozen water is diagnostically determined as a function of
137 temperature. Cloud water is in the liquid phase when temperature is 0°C or higher. Fraction of
138 frozen water monotonically increases (and fraction of liquid water decreases) with decreasing
139 temperature towards -23°C, and only frozen water can occur in the reanalysis in conditions with
140 temperature below -23°C. It is, however, noteworthy that in observations from Alaska, northern
141 Canada, and the western Arctic Ocean, liquid water has been found in clouds at temperatures as
142 low as -40°C (Shupe 2011).

143 Accuracy of ERA-Interim data and its impacts on the results of this study is discussed in the
144 Supplemental material. In summary, the accuracy of ERA-Interim can be considered as sufficient
145 when it comes to an investigation of relationships between atmospheric large-scale circulation,
146 and moisture and cloud distributions. The main focus of this study is on anomalies. Anomalies
147 are considered as more trustworthy than mean values (Liu and Key 2016), although anomalies
148 are also liable to notable uncertainties in their response to large-scale circulation, due to possible
149 misrepresentation of physical processes related to clouds and turbulence in the reanalysis. We
150 presume that the largest uncertainties in this study are related to cloud phases, and we are
151 therefore careful for not drawing too far conclusions based on the cloud phase.

152 **b. The Self-Organizing Map method**

153 Generalized atmospheric circulation patterns in the Arctic, obtained by applying the SOM
154 statistical clustering method, form the core of this study. The SOM method was developed by
155 Kohonen (2001), and it can be characterized as a non-linear mapping of high-dimensional input

156 data onto a two-dimensional array of reference vectors, i.e. nodes. In other words, the method
157 uses unsupervised learning to determine generalized patterns in data. The SOM method has
158 originally been developed for artificial neural networks, but it has been extensively applied in
159 many fields of science; since 2002 also in climatology of synoptic patterns (Hewitson and Crane
160 2002). The first SOM study addressing the Arctic was published by Cassano et al. (2006) who
161 derived a synoptic climatology for the Arctic from an ensemble of twenty and twenty-first century
162 climate simulations. More recently, SOMs have been utilized to for example assess future
163 changes in meridional moisture transport across 70°N (Skific et al. 2009) and to classify
164 atmospheric moisture transport pathways in the vicinity of Greenland Ice Sheet (Mattingly et al.
165 2016). The SOM method is a statistical method, not a physical-based method, but it has
166 demonstrated its ability to cluster similar pressure patterns in a physically meaningful way in
167 previous studies.

168 In this study, the method provides a two-dimensional array of gridded MSLP fields, which have
169 the main characteristics of the input MSLP data. The method preserves the probability density of
170 the input data by allocating more nodes to more frequent patterns in the input data (Cassano et
171 al. 2006). The size of node array is often subjectively determined by user. The size depends on
172 the application; fewer nodes will lead to a high level of generalization of the patterns but make
173 the visualization and conceptualization of the results easier, whereas more nodes will increase
174 the level of details and amount of regional features in the patterns (Hewitson and Crane 2002).

175 First, an initial array of reference vectors is created by the SOM algorithm procedure. Each node
176 has an associated reference vector which has equal dimensions to the input data. For example,

177 if the input data are a time series in a 2-dimensional spatial grid of 50 x 50, each node will have
178 a reference vector consisting of 2500 values. The initialization can be made in several ways, but
179 in this study, we applied the random initialization scheme, in which the initial reference vectors
180 are randomly selected. Second, during the training each data vector constituted by each time
181 step of the input data is compared with the reference vector of each node. Depending on the
182 similarity between the data and reference vectors, measured as the Euclidian distances, the
183 reference vectors of the SOM are adjusted towards the data vectors. The node having the most
184 similar reference vector to a data vector is adjusted most, and the nodes around it, within a user-
185 defined radius, are also adjusted but to a lesser degree depending on their distance from the
186 most-adjusted node (Cassano et al. 2006). The degree of adjustment is defined by a user-defined
187 learning-rate parameter. The procedure is repeated until the Euclidian distances of reference
188 vectors to the input data do not change and are hereby minimized. Finally, reference vectors
189 become ordered despite the fact that they were initially randomly distributed. In the resulting
190 SOM array, similar patterns are located close to each other whereas dissimilar patterns are
191 located far apart. Each time step of the input data can then be associated to the most similar
192 node based on the Euclidian distance.

193 In this study, the SOM method was applied to 15 years (2003–2017) of wintertime (DJF) MSLP
194 data of ERA-Interim at 6 h interval. To ensure equal weighting in the whole study region, the
195 MSLP data were first re-gridded to an equal-area grid. Based on a subjective evaluation, 5 x 6
196 array of nodes was selected as the most appropriate to represent wintertime atmospheric
197 circulation patterns in the Arctic. It was found out that as many as 30 different circulation regimes
198 were needed to adequately resolve details of different circulation patterns because much of the

199 horizontal moisture transport is typically driven by narrow, filamentary moisture intrusions.
200 Moisture, cloud and radiation variables were associated with circulation regimes based on their
201 time steps, and anomalies were calculated by combining the time steps belonging to a certain
202 node. The anomalies were calculated by subtracting the grid-point mean values for the time steps
203 belonging to a certain node from the grid-point mean values for the whole time series.

204 **c. Horizontal moisture transport**

205 In addition to variables available in ERA-Interim, we also show results for horizontal moisture
206 transport. Horizontal moisture transport, calculated on each pressure level of ERA-Interim from
207 the surface to 300 hPa, was divided into meridional transport

208 $f_v = qv$ (1)

209 and zonal transport

210 $f_u = qu$ (2)

211 where q is specific humidity, v is meridional wind component and u is zonal wind component.
212 Vertically integrated moisture transport from the surface to the 300-hPa level F_v was obtained
213 for the meridional component in a discrete form as follows:

214

$$215 F_v = \int_{p_{surface}}^{300 \text{ hPa}} \frac{1}{g} qv dp \approx \sum_{i=1}^{n-1} \frac{1}{2g} (q_i v_i + q_{i+1} v_{i+1}) (p_i - p_{i+1}),$$

(3)

216 where p is air pressure, g is the gravitational acceleration and subscript i refers to the index of
217 each pressure level ($i=1$ corresponds to the surface). Levels below the surface were not included
218 in the calculations; the levels were removed from the analysis if the pressure at the level was
219 higher than the actual surface pressure at that particular time step. Below the lowest pressure
220 level (located above the surface), the flux density of the lowest pressure level was used for the
221 layer between that level and the surface. The zonal component of the vertically integrated
222 moisture transport was calculated by replacing v with u in Eq. 3. Following Naakka et al. (2019),
223 who stated that northward and southward transports partly compensate each other in the net
224 horizontal transport, we also show results for the total moisture transport. The total meridional
225 transport is defined as a mean of the absolute values of the instantaneous meridional transports,
226 and it therefore better represents the actual moisture transport taking place without the impact
227 of compensation.

228 When anomalies of moisture, cloud and radiation variables were associated with circulation
229 regimes of SOM, statistical significance of these anomalies was tested by applying a Monte Carlo
230 approach. This was done by constructing 5000 random subsets of a given field from the original
231 data and comparing anomalies in the random subsets to the anomalies in the SOM nodes. The
232 subsets had the same number of samples as the SOM nodes. Then, a two-tailed test was
233 performed. In a given grid point, if less than 1% of the anomalies in the random subsets were
234 higher than the anomaly in the original SOM node or less than 1% of the anomalies in the random
235 subsets were lower than the anomaly in the SOM node, the anomaly was different from zero at
236 the 98% significance level. For regional anomalies, the Monte Carlo approach was applied to
237 regionally averaged anomaly values, instead of grid-point values, but the principle was otherwise

238 the same. Regionally averaged anomalies are shown for six sub-regions: 1) the Arctic Ocean, 2)
239 The North Atlantic, 3) Northern Europe, 4) Siberia, 5) Alaska and Canada, and 6) Greenland (Fig.
240 1). The division of regions is adapted from Naakka et al. (2018), who defined these based on
241 spatial patterns of specific humidity.

242 **d. Circulation indices**

243 The circulation patterns, as well as moisture and cloud variables, were related to indices of the
244 AO, NAO and to Greenland Blocking Index (GBI), and to a frequently occurring pressure pattern,
245 described in Section 3b. The AO is the leading empirical orthogonal function of wintertime sea-
246 level pressure field. It is a large-scale mode of climate variability in the Northern Hemisphere
247 which displays an opposing pattern of pressure between the Arctic and the mid-latitudes
248 (Thompson and Wallace 1998). In the negative phase of the AO, the zonal flow is weaker than
249 usual and the meridional flow is enhanced, whereas the positive phase is associated with a
250 relatively strong zonal flow. The NAO, in turn, consists of a north-south dipole of pressure
251 anomalies between the Azores subtropical high and the Icelandic subpolar low (Barnston and
252 Livezey 1987). The positive phase of the NAO is associated with a northward shift of North
253 Atlantic storm tracks whereas the negative NAO phase is associated with weaker westerly winds.
254 The NAO correlates to a high degree with the AO. In this study, daily values of the AO and NAO
255 were obtained from the websites of Climate Prediction Center of National Oceanic and
256 Atmospheric Administration (NOAA)
257 (http://www.cpc.ncep.noaa.gov/products/precip/CWlink/daily_ao_index/ao.shtml) and
258 (<http://www.cpc.ncep.noaa.gov/products/precip/CWlink/pna/nao.shtml>). GBI is a measure of

259 blocking in Greenland, defined as the mean 500 hPa geopotential height for the 60–80°N, 20–
260 80°W area, and it emphasizes more the northern center of the NAO dipole pattern (Hanna et al.
261 2013). Daily values of GBI were obtained from Earth System Research Laboratory of NOAA
262 (https://www.esrl.noaa.gov/psd/gcos_wgsp/Timeseries/GBI_UL). All daily index values were
263 linearly interpolated to 6-hour intervals in order to associate them with the SOM regimes of the
264 same time intervals.

265 **3. Results**

266 **a. Mean distributions of moisture and clouds**

267 In this Section, an overview of mean moisture and cloud distributions in the Arctic in winter
268 (2003–2017) is given. These results will enable relating the anomalies presented in Section 3c to
269 mean values of the variables.

270 According to ERA-Interim, the Arctic is generally cloudy in winter, and especially the low-level
271 cloud fraction is high (Fig. 2a–c). The regional differences in cloud fraction at low, medium and
272 high levels are not dramatic, but the mean fields hide a bi-modal cloud fraction distribution,
273 peaking at clear-sky (fraction < 0.1) and overcast conditions (fraction > 0.9) (Fig. 2d–f). Overcast
274 conditions are most common at the low level. Clear-sky conditions are most common at the
275 medium and high levels where their occurrence is approximately 50%.

276 Interestingly, mean spatial distribution of cloud water in winter (Fig. 3a–c) does not resemble the
277 spatial distribution of cloud fraction (Fig. 2a–c), but rather resembles the mean distribution of
278 water vapor (Fig. 3d). The spatial maxima of vertically integrated total cloud water are found in

279 the North Atlantic and the Gulf of Alaska, particularly in the vicinity of high orography. In the
280 Arctic Ocean, Siberia, North America and Greenland, the water vapor and cloud water content
281 are relatively low and the cloud condensate mainly occurs in the frozen phase in ERA-Interim.
282 The mean spatial distribution of total cloud water (Fig. 3c) is, to some extent, also similar to the
283 distributions of net meridional moisture transport (Fig. 3f) and evaporation (Fig. 3e); evaporation
284 has its maxima in the ice-free ocean areas, whereas meridional moisture transport peaks are
285 more defined to the North Atlantic and the Gulf of Alaska.

286 Mean vertical profiles of moisture and cloud variables have notable regional variability, but the
287 mean profiles of different variables seem to be connected to each other in a similar way in all of
288 the regions (Fig. 4). The shapes of specific humidity profiles are very similar to the profiles of total
289 meridional moisture transport (the sum of absolute northward and southward transports),
290 having the vertical maximum at the same level as the total meridional transport or, at the most,
291 50 hPa lower. Humidity inversions, i.e., layers in which the specific humidity increases upwards,
292 are visible in the profiles of specific humidity, except in the North Atlantic, where the specific
293 humidity maximum is at the surface, presumably due to large evaporation from the sea surface
294 in this region. On one hand, the specific humidity maxima aloft are at least partly a cause of
295 vertically uneven horizontal moisture transport, having the maximum between 900–800 hPa; on
296 the other hand, the specific humidity inversion probably contributes to the vertical profile of the
297 moisture transport maintaining its elevated maximum. Due to compensating effects of
298 northward and southward transport, the net meridional moisture transport profiles have less
299 pronounced variability with height than the total transport. Cloud water basically peaks at the
300 same altitude as the total moisture transport and specific humidity, except in the North Atlantic

301 where the large sensible heat flux from the warm ocean leads to efficient mixing in the boundary
302 layer, reducing the relative humidity near the surface but leading to condensation higher in the
303 well-mixed layer. Profiles of cloud fraction have independent characteristics and do not directly
304 match with the moisture and cloud water profiles. Large spatial variability in both horizontal and
305 vertical directions is also evident in cross sections of cloud water content at 60°N and 70°N (Fig.
306 5). Cross sections of net moisture transport in ERA-Interim are not shown here because they have
307 previously been presented by Naakka et al. (2019) (in their Fig. 10) nearly for the same period
308 (2003–2014). The general characteristics of cross sections of net moisture transport and cloud
309 water content are similar. For example, large amounts of cloud water occur in a high column in
310 the North Atlantic and the Gulf of Alaska, in areas where the net meridional moisture transport
311 is also large according to Naakka et al. (2019). High mountains act as division lines for moisture
312 transport and cloud water content, and alter the height of cloud water maximum. An example of
313 this can be seen at 60°N in Fig. 5c, in which cloud water in the North Atlantic (from 45°W to 0°)
314 occurs over a large vertical range having the maximum around 850 hPa level, whereas the cloud
315 water maximum on the eastern side of Norwegian mountains (from 20°E to 60°E) is located at 75
316 hPa lower. At 70°N, most of the cloud water is found between 30°W and 90°E, across the
317 Greenland and Norwegian Sea and parts of Northern Europe. Liquid cloud water is mostly limited
318 to levels below 800 hPa.

319 **b. Large-scale circulation regimes**

320 Wintertime atmospheric circulation in the Arctic was condensed to 30 types of circulation
321 regimes applying the SOM method (Section 2b). Each time step of our data is designated to one

322 of these circulation regimes. The circulation types are presented in a 5 x 6 array in which the most
323 similar regimes are located close to each other. The array of the characteristic MSLP patterns is
324 shown in Fig. 6, and corresponding array of MSLP anomaly patterns is shown in Fig. S1. Note that
325 the MSLP patterns shown in Figs. 6 and S1 are the mean values of MSLP over the time steps
326 belonging to each node, and hence they are not the reference vectors directly provided by the
327 SOM algorithm. The relatively small difference (root-mean-square difference of 10 hPa) between
328 the node-mean MSLP patterns and the reference vectors provided by the SOM method is an
329 indicator that the regimes provided by the SOM algorithm are representative statistical
330 constructs, which are not overly generalized.

331 All of the circulation regimes have at least 76 samples (i.e., 1.4% of the time steps) in them (Fig.
332 6). The corner circulation regimes 26 and 5 as well as regime 15 are the most common ones. The
333 nodes 5 and 15 are characterized by anomalously low pressure in Northern Eurasia, whereas
334 regime 26 is characterized by anomalously high pressure in the most of the Arctic. Regime 30,
335 with anomalously high pressure in Northern Europe and western parts of Russia, is clearly the
336 most persistent regime with its mean persistence of 3.8 days. In all of the regimes, transitions
337 from one regime to another most commonly take place between the neighbouring or diagonally
338 closest regimes in the array.

339 Mean values of AO and NAO indices for each SOM node are shown in Fig. 7a–b. The circulation
340 regimes in the three uppermost lines of the SOM array (nodes 1–15) are mostly associated with
341 positive phases of these modes, whereas the corner node 26 and nodes around it are associated
342 with negative phases of AO and NAO. In the circulation regimes linked with positive AO and NAO,

343 the MSLP field is characterized by anomalously low pressure in one or several areas in the
344 subpolar latitudes, typically in the North Atlantic and/or where the Aleutian Low is reaching far
345 north (Figs. 6 and S1). In negative phases of AO and NAO, positive anomalies of MSLP occur in
346 the most of the Arctic, especially in the Arctic Ocean, northern Eurasia and Greenland. GBI is
347 strongest in negative phases of AO and NAO, but also when the subpolar low pressure in the
348 European sector is relatively weak or located far to the east from Greenland (in the rightmost
349 column of the array) (Fig. 7c).

350 In addition to above-mentioned indices, we define ‘Arctic Bridge’ based on a frequently occurring
351 circulation pattern which has clear impacts on the moisture and cloud distributions in the Arctic.
352 The Arctic Bridge is qualitatively defined here as a continuous high pressure reaching from Siberia
353 to Northern America through the Arctic Ocean, with no isobars crossing from the Atlantic sector
354 to the Pacific sector. The Arctic Bridge prevents a flow from the Atlantic sector to reach the
355 Pacific. The Arctic Bridge is present in 22 of the circulation regimes, and its strength in those
356 circulation regimes is subjectively evaluated from Fig. 6 to be either strong or weak (Fig. 7d).
357 Occurrence of the Arctic Bridge is neither directly linked to the indices of AO and NAO, nor that
358 of GBI.

359

360 **c. Linkages to moisture, clouds and downward longwave radiation**

361 Relationships between large-scale circulation regimes and moisture and cloud properties are
362 evident. To illustrate this, anomalies of horizontal moisture transport, water vapor, cloud water

363 and downward longwave radiation at the surface are shown in Fig. 8 for four regimes (1, 5, 26,
364 and 30). Corresponding distributions of divergence of the horizontal moisture transport,
365 anomalies of evaporation and medium level cloud fraction in the same four SOM nodes are
366 shown in Fig. S2. These regimes are located in the corners of the SOM and hence, they represent
367 the most different circulation regimes which are also among the most common ones. The four
368 example regimes demonstrate the general relationships between variables, which are also
369 commonly found in the other circulation regimes. Most of the anomalies related to different
370 circulation regimes, and discussed in the following paragraphs, are statistically significant at 98%
371 level, which is indicated in the figures. In addition, anomalies of horizontal moisture transport,
372 cloud water and downward longwave radiation in all of the 30 circulation regimes are shown in
373 the Supplemental material (Figs. S3–S5) to provide detailed information on different circulation
374 types and their regional impacts.

375 The circulation of regime 1 is characterized by anomalously high pressure over Alaska,
376 anomalously low pressure in the western part of North Atlantic and a presence of strong Arctic
377 Bridge, and it is linked to the positive phase of NAO and AO (Figs. 6, S1 and 7). As seen in Fig. 8,
378 this circulation pattern enables increased meridional moisture transport in the regions where the
379 zonal pressure gradients are large, resulting in enhanced northward moisture transport in the
380 North Atlantic and around the Bering Strait, and strong negative anomaly in the transport in the
381 western parts of the North America and on the coasts of Greenland. In this circulation type,
382 moisture is simultaneously transported to the central Arctic both from the Atlantic and Pacific
383 Ocean, and these two moisture paths are separated by the Arctic Bridge. In the two regions of
384 anomalously strong northward moisture transport, the vertically integrated water vapor has also

385 anomalously high values. Impacts of the zonal moisture transport component can also be seen,
386 especially in Alaska and on the east side of Greenland. On one hand, the high water vapor is a
387 consequence of increased moisture transport to the area, while, on the other hand, it is the high
388 water vapor content that enables the large moisture transport to take place in the area.
389 Evaporation, in turn, has negative anomalies in the regions where there is a high amount of water
390 vapor and large northward transport (Fig. S2), which is presumably explained by the reduction of
391 evaporation when the air above the surface is relatively moist.

392 In regime 1, anomalies of cloud water are to a large extent co-located with those of water vapor,
393 although the cloud anomalies show more small-scale variability in space. A closer look at the east
394 coast of Greenland shows that there is a pronounced positive cloud water anomaly, mainly in the
395 frozen phase, which has a large vertical extent reaching nearly from the surface to 700 hPa (Figs.
396 8 and 9). Thus, Greenland is acting as a cold barrier for transported moisture which leads to
397 enhanced condensation and amounts of cloud water on the coast (via water vapor convergence,
398 shown in Fig. S2, condensation due to lifting of the air mass, and impacts of the cold surface of
399 Greenland), and a similar effect of Greenland is seen in all of the SOM nodes in which the flow
400 has a perpendicular component towards the coast of Greenland. The match between moisture
401 convergence and cloud water is also very good in the Pacific sector (Figs. 8 and S2). In the vertical
402 direction, anomalies of meridional moisture transport and cloud water are not exactly co-located
403 (Fig. 9); cloud water anomalies have maxima higher up in the atmosphere than the meridional
404 moisture transport, reflecting an influence of the vertical profiles of temperature on cloud
405 condensation. Medium cloud cover anomaly field (Fig. S2) resembles the cloud water
406 distribution, but the cloud cover anomalies are weaker and less commonly statistically significant.

407 Low level cloud cover is rather independent from the cloud water distribution (not shown). The
408 anomaly field of downward longwave radiation at the surface is almost directly a composite of
409 water vapor and cloud water anomaly fields (Fig. 8), although temperature of the air masses also
410 influences the downward longwave radiation.

411 The circulation in regime 5 is characterized by anomalously high pressure over North America,
412 anomalously low pressure in the whole Eurasia, the positive phase of AO and NAO, and the
413 existence of weak Arctic Bridge (Figs. S1 and 7). In most of Eurasia, the flow is very zonal, and in
414 the northern part of the North Atlantic, the meridional component of moisture transport is
415 directed southwards, prohibiting moisture transport from the North Atlantic towards higher
416 latitudes. Thus, moisture transport to the Arctic is mainly taking place through the area of the
417 Bering Strait. The vertically integrated water vapor is anomalously high in the vicinity of Bering
418 Strait, linked to the large moisture transport. Evaporation has a positive anomaly in the North
419 Atlantic, i.e., in the same region with large negative anomalies of meridional moisture transport
420 and water vapor (Fig. S2). It is noteworthy that the flow in this region, and not only its anomaly,
421 is directed southwards and hence the moisture provided by evaporation is transported towards
422 lower latitudes. This is practically the case for positive anomalies of evaporation in all of the
423 circulation regimes, so that anomalously high evaporation is linked to a southward flow.
424 Anomalies of vertically integrated cloud water and downward longwave radiation resemble the
425 water vapor anomaly distribution, but, in addition, show a small area with a pronounced positive
426 anomaly on the west coast of Norway due to convergence of horizontal moisture transport (Fig.
427 S2). Interestingly, the negative anomaly of cloud water in the North Atlantic is not associated to
428 a reduced medium (or low) cloud cover in this region (Fig. S2).

429 The dominating feature in the circulation in regime 26, the most frequent of all the regimes, is
430 an anomalous high pressure situated over the central Arctic and Greenland (Figs. 6 and S1). This
431 extensive high pressure drastically reduces the meridional moisture transport to high latitudes.
432 This circulation type also causes a large negative anomaly for zonal transport, although the zonal
433 transport is still weakly eastward at most of the longitudes along 60°N. The regime is associated
434 with the largely negative AO and NAO, strong Arctic Bridge, and it has the highest GBI of all the
435 regimes (Fig. 7). Regime 26 is one of the circulation regimes in which the northward moisture
436 transport is strongest on the west side of Greenland. This northward transport is presumably
437 causing statistically significant positive anomalies of water vapor, cloud water and downward
438 longwave radiation in the region and farther north (Figs. 8 and S3). In the North Atlantic and the
439 most of Northern Eurasia, the regime is linked to large negative anomalies in moisture transport,
440 water vapor, cloud water and downward longwave radiation, but not in low and medium cloud
441 cover. This statistically significant negative anomaly of cloud water content reaches at least up
442 to 300 hPa (Fig. 9).

443 Circulation regime 30 is characterized by anomalously high pressure over Eurasia, and weak
444 negative pressure anomalies over North America and the Canada Basin (Figs. 6 and S1). This
445 circulation regime has clearly the highest persistency of all the regimes (Fig. 6). The regime is
446 associated with the negative AO but positive NAO, and, importantly, it is one of the eight regimes
447 in which the Arctic Bridge does not exist (Fig. 7). The lack of Arctic Bridge has large impacts on
448 moisture and clouds, especially, at latitudes north of 70°N, as it allows the horizontal moisture
449 transport from the North Atlantic to the Pole and farther towards the Bering Strait. In some of
450 the circulation regimes, like in 19 and 24, the moisture from the North Atlantic flows over the

451 Pole all the way to the Bering Strait (Fig. S3). In regime 30, however, moisture is transported
452 along the large pressure gradient towards the Barents, Kara and Laptev seas (Fig. 8), from where
453 this moist air mass is moving back towards lower latitudes, seen as a negative anomaly of
454 meridional moisture transport. The horizontal path of the moisture is associated with positive
455 anomalies in water vapor, cloud water and downward longwave radiation, and anomalously little
456 evaporation (Figs. 8 and S2). Along this path, phase changes occur from liquid to frozen water.
457 An indication of these phase changes is that positive anomalies of liquid water in regime 30 are
458 mainly limited to the North Atlantic, whereas positive anomalies of frozen water are found
459 farther along the path, over the central Arctic Ocean as well as over Barents, Kara and Laptev
460 seas (not shown). Direct impacts of the high pressure, presumably related to the potential drying
461 effect of large-scale subsidence and lack of efficient moisture transport, are seen in the Northern
462 Europe and western part of Russia as an anomalously low water vapor content, cloud water
463 content, medium- and high-level cloud cover and downward longwave radiation (Figs. 8 and S2).

464 Relationships between moisture and cloud variables and the circulation regimes do not directly
465 indicate causality. To further address how moisture anomalies progress in time, time lead and
466 lag were investigated in the circumpolar Arctic between 70°N and 80°N, by setting the start time
467 of each circulation regime to zero at the day this circulation regime occurs. Time lag for anomaly
468 of vertically integrated water vapor is shown in Fig. 10 for the four corner circulation regimes.
469 Results for cloud water were qualitatively similar, but had more small scale variability in time and
470 space (not shown). In regime 1, the positive water vapor anomaly in the North Atlantic is mainly
471 initiated by the regime, which is indicated by the maximum for positive time lags. The magnitude
472 of the positive anomaly stays nearly constant for the following 72 hours, and spreads in the zonal

473 direction with time. The positive anomaly around the Bering Strait in regime 1 and the positive
474 anomaly in the North Atlantic in regime 30, are typically not initiated but rather intensified by
475 these regimes. This manifests that these regimes typically occur after a regime which is also
476 related to positive, but weaker, anomalies in the region; most commonly regime 6 with a strong
477 positive anomaly in the Bering Strait precedes regime 1, and regime 29 with positive anomaly in
478 the northern part of North Atlantic precedes regime 30 (not shown). The negative anomalies in
479 the North Atlantic in regimes 5 and 26 are drastically intensified after the start of these regimes,
480 although the typically preceding regimes are also linked to negative anomalies in the region. The
481 time lag analyses suggest that the anomalies of water vapor (and cloud water) are responding to
482 atmospheric circulation, but confirming the actual causality would require for instance some
483 sensitivity experiments with a numerical model.

484 Regional impacts of the circulation regimes are illustrated with regional anomaly arrays for the
485 meridional moisture transport, as well as vertically integrated water vapor and cloud water
486 (Fig.11). The region definitions are shown in Fig. 1. Positive and negative anomalies are clustered
487 in the arrays, but positions and orientations of these clusters naturally vary from region to region,
488 because each region has individual pressure patterns as a part of a circulation regime. Impacts of
489 the AO and NAO are directly seen in the anomaly arrays of Northern Europe and Greenland, but
490 in opposite ways. In Northern Europe, circulation regimes related to the positive (negative) AO
491 and NAO are associated with positive (negative) anomalies of meridional moisture transport,
492 water vapor and cloud water, but in Greenland the positive AO and NAO are linked with negative
493 anomalies of these variables. In Siberia, positive moisture and cloud anomalies are typically
494 associated with negative anomalies in the regional MSLP. In the North Atlantic, circulation

495 regimes situated diagonally, from regime 1 to 30, in the array are associated with positive
496 moisture and cloud anomalies. A common denominator for these diagonally situated regimes is
497 the northward directed flow in the North Atlantic, but otherwise these regimes differ largely.

498 **4. Discussion and conclusions**

499 Largest anomalies of moisture transport related to certain circulation regimes are as large as the
500 mean net moisture transport itself. In addition, anomalies of water vapor are often up to $\pm 3 \text{ kg}$
501 m^{-2} , and anomalies of cloud water up to 80 g kg^{-1} , which are in many regions comparable to the
502 mean values of these variables (Fig. 3). Anomalies of downward longwave radiation are in many
503 circulation regimes up to $\pm 50 \text{ W m}^{-2}$, which may strongly influence the surface temperature. It is
504 important to acknowledge the large uncertainties especially in cloud water and downward
505 longwave radiation, which may affect the anomalies but are estimated to be smaller in
506 magnitude than the anomalies reported (see Supplemental material). Effects of large-scale
507 circulation on spatio-temporal distributions of water vapor, cloud water and longwave radiation
508 in the Arctic are to a large extent occurring through the impact of horizontal moisture transport.
509 In the horizontal direction, distribution of moisture transport largely defines the distributions of
510 water vapor and cloud water. Convergence of moisture transport influences the spatial
511 distributions of cloud water mainly when the flow has a component toward a high orography,
512 causing positive anomalies of cloud water, reaching high altitudes over the coasts of Greenland,
513 Norway and Alaska. It appears that relatively weak convergence can lead to an anomalously large
514 amount of cloud water; it seems that it is enough to have a positive anomaly in water vapor and
515 a sufficient amount of convergence. Furthermore, anomalies in moisture transport and moisture

516 convergence are not totally independent. Theoretically moisture transport occurs along moist
517 isentropes which typically are tilted upwards towards the north and hence moisture transport
518 commonly occurs with upward motion of air leading to enough moisture convergence to form
519 clouds. In the vertical direction, cloud water distribution is shaped by the profiles of both
520 moisture transport and temperature. In high-pressure regions, the absence of effective moisture
521 transport (together with subsidence which can potentially further dry the air) is seen as negative
522 anomalies of specific humidity, cloud water content, and downward longwave radiation. On one
523 hand, the results emphasize the importance of horizontal moisture transport in the climate
524 system of the Arctic in winter, as also indicated in several previous studies, e.g., by Curry and
525 Herman (1985), and Liu et al. (2018). On the other hand, cloud cover, in particular low-level cloud
526 cover, in ERA-interim, seems to match rather poorly with the moisture, cloud water and
527 downward longwave radiation distribution, which might depend on the parameterization of the
528 physical processes and model resolution. Hence, thin, even uniform, cloud cover can be
529 associated with a variety of meteorological situations, whereas anomalously high cloud water
530 content is typically dependent on the moisture transport. Especially, the poor match between
531 the anomalies of low clouds and downward longwave radiation at the surface is rather surprising,
532 because the low cloud cover typically has a larger radiative influence on the surface than the
533 middle and high level clouds.

534 Evaporation is a source of moisture over the partially ice-free oceans in winter, but it is typically
535 not efficient enough to shape the large-scale distributions of specific humidity and cloud water
536 in the synoptic scale. Positive anomalies in evaporation are found when the flow is directed
537 southward (typically associated with cold-air outbreaks), meaning that much of the moisture

538 provided by the evaporation taking place in the Arctic is in fact transported southwards, and not
539 towards higher latitudes. Evaporation may still be very important in winter for Arctic clouds
540 locally (Curry et al. 1996), and long-term changes in evaporation have been reported to have an
541 impact on cloud formation and longwave radiation (Jun et al. 2016).

542 Many of the impacts of large-scale circulation on moisture, clouds and longwave radiation are
543 associated to frequently occurring large-scale pressure patterns. Previously, Groves and Francis
544 (2002) have reported larger northward moisture transport across 70°N over the Atlantic sector
545 and larger southward moisture transport over the Canadian Archipelago when the AO is strongly
546 positive. Devasthale et al. (2012) has reported a similar dipole structure in cloud fraction
547 anomalies eastward and westward of Greenland, shifting between the opposite states depending
548 on the sign of AO. Our results are in line with these previous findings, but provide more
549 comprehensive evidence on the impacts of AO on cloud distributions through various
550 atmospheric circulation patterns and their associated moisture transport. Similarly to the
551 previous studies, our results indicate that in the Northern Europe and eastern North Atlantic,
552 circulation regimes related to the positive (negative) AO are typically associated with positive
553 (negative) anomalies of meridional moisture transport, water vapor and cloud water. In western
554 North Atlantic, Greenland and the Canadian archipelago the positive AO is linked to negative
555 anomalies of these variables. We also show a similar dipole structure in relation to the NAO.
556 However, our study also shows that a single value of NAO/AO index can hide very different
557 circulation patterns which in turn have large impacts on the regional moisture transport in the
558 Arctic. For example, positive phases of the AO and NAO include commonly occurring circulation
559 regimes in which the dipole structure in the North Atlantic is not present, but, instead, the

560 meridional transport is anomalously positive around the Bering Strait, as in the circulation regime
561 5 (Figs. 6 and 8). Except for studies addressing the reasons for the sea ice minimum in summer
562 2007 (L'Heureux et al. 2008; Graversen et al. 2011), the strong meridional transport from the
563 Pacific has received less attention than transport from the Atlantic sector. Strong Greenland
564 blocking, in turn, typically causes a positive anomaly in water vapor, cloud water and downward
565 longwave radiation in the southwest of Greenland and negative anomalies in these variables in
566 the North Atlantic.

567 In this study, we qualitatively defined a frequently occurring circulation pattern, the Arctic Bridge,
568 which is a continuous high-pressure pattern reaching from Siberia to Northern America through
569 the Arctic Ocean. The Arctic Bridge prevents a flow from the Atlantic to reach the Pacific sector.
570 If the Arctic Bridge does not exist, horizontal moisture transport from the North Atlantic across
571 the central Arctic Ocean may occur, and positive anomalies of specific humidity, cloud water and
572 downward longwave radiation are often seen near the Pole and along the path of the flow
573 towards the Bering Strait. Especially, the results suggest that those circulation regimes lacking
574 the Arctic Bridge are subjected to a long fetch over the sea ice and long exposure for effective
575 radiative cooling at high latitudes, which presumably leads to air-mass modification and phase
576 changes along the flow; these phase changes in clouds have been indicated as very important for
577 radiative effects of clouds and for cloud decay and dissipation (Pithan et al. 2018).

578 Our results reveal a high dependence of moisture and cloud variables on atmospheric pressure
579 fields, which appears important in the climate change perspective. In the future, changes in
580 pressure fields, for example related to the sea ice loss (Screen et al. 2018), could potentially

581 largely modify the moisture transport in the Arctic, and thereby also modify regional distributions
582 of water vapor, cloud water and downward longwave radiation, at least regionally. Sea ice loss
583 could possibly modify the frequency and duration of certain circulation patterns, and hence also
584 the moisture transport related to each circulation pattern. For the net moisture flux across 70°N
585 during the twenty-first century, it has been suggested that the projected increase will be more
586 attributed to factors related to thermodynamic effects rather than changes in the circulation
587 patterns (Skific et al. 2009). Projections on future changes in the Arctic clouds have remained as
588 a major challenge for the scientific community; different modelling studies have yielded
589 contrasting results (Vavrus et al. 2012; Koenigk et al. 2013). This study emphasizes that future
590 changes in Arctic clouds are to be expected in connection with the projected enhanced
591 meridional moisture transport into the Arctic.

592 **Acknowledgements**

593 The study was supported by the Academy of Finland via projects TODAy (308441) and AFEC
594 (317999). R. G. Graversen was supported by the Research Council of Norway (280727), and P.
595 Uotila by the EU MCSA grant (707262-LAWINE). We thank P. Gibson for providing the R code for
596 the SOM analyses. The computations were partly accomplished on the supercomputer Stallo at
597 University of Tromsø under the Norwegian Metacenter for Computational Science (NOTUR)
598 (projects NN9348K and NS9063K)

599 **References:**

- 600 Barnston, A. G., and R. E. Livezey, 1987: Classification, Seasonality and Persistence of Low-
601 Frequency Atmospheric Circulation Patterns, *Mon. Weather Rev.*, **115**, 1083-1126,
602 doi:10.1175/1520-0493(1987)115<1083:csapol>2.0.co;2.
- 603 Boisvert, L. N., D. L. Wu, and C.-L. Shie, 2015: Increasing evaporation amounts seen in the Arctic
604 between 2003 and 2013 from AIRS data, *J. Geophys. Res. Atmos.*, **120**, 6865-6881,
605 doi:doi:10.1002/2015JD023258.
- 606 Cassano, J. J., P. Uotila, and A. Lynch, 2006: Changes in synoptic weather patterns in the polar
607 regions in the twentieth and twenty-first centuries, part 1: Arctic, *Int. J. Climatol.*, **26**,
608 1027-1049, doi:doi:10.1002/joc.1306.
- 609 Curry, J. A., and G. F. Herman, 1985: Relationships between Large-Scale Heat and Moisture
610 Budgets and the Occurrence of Arctic Stratus Clouds, *Mon. Weather Rev.*, **113**, 1441-
611 1457, doi:10.1175/1520-0493(1985)113<1441:rblsha>2.0.co;2.
- 612 Curry, J. A., W. B. Rossow, D. Randall, and J. L. Shramm, 1996: Overview of Arctic Cloud and
613 Radiation Characteristics, *J. Clim.*, **9**, 1731–1764.
- 614 Dee, D. P. and Coauthors, 2011: The ERA-Interim reanalysis: configuration and performance of
615 the data assimilation system, *Quart. J. Roy. Meteorol. Soc.*, **137**, 553–597,
616 doi:10.1002/qj.828.
- 617 Devasthale, A., M. Tjernström, M. Caian, M. A. Thomas, B. H. Kahn, and E. J. Fetzer, 2012:
618 Influence of the Arctic Oscillation on the vertical distribution of clouds as observed by
619 the A-Train constellation of satellites, *Atmos. Chem. Phys.*, **12**, 10535-10544,
620 doi:10.5194/acp-12-10535-2012.

- 621 Doyle, J. G., G. Lesins, C. P. Thackray, C. Perro, G. J. Nott, T. J. Duck, R. Damoah, and J. R.
622 Drummond, 2011: Water vapor intrusions into the High Arctic during winter, *Geophys.*
623 *Res. Lett.*, **38**, doi:10.1029/2011GL047493.
- 624 Dufour, A., O. Zolina, and S. K. Gulev, 2016: Atmospheric Moisture Transport to the Arctic:
625 Assessment of Reanalyses and Analysis of Transport Components, *J. Clim.*, **29**, 5061-
626 5081, doi:10.1175/JCLI-D-15-0559.1.
- 627 Eastman, R., and S. G. Warren, 2010: Interannual Variations of Arctic Cloud Types in Relation to
628 Sea Ice, *J. Clim.*, **23**, 4216-4232, doi:10.1175/2010jcli3492.1.
- 629 Gimeno-Sotelo, L., R. Nieto, M. Vázquez, and L. Gimeno, 2018: A new pattern of the moisture
630 transport for precipitation related to the drastic decline in Arctic sea ice extent, *Earth*
631 *Syst. Dynam.*, **9**, 611-625, doi:10.5194/esd-9-611-2018.
- 632 Gong, T., S. Feldstein, and S. Lee, 2017: The Role of Downward Infrared Radiation in the Recent
633 Arctic Winter Warming Trend, *J. Clim.*, **30**, 4937-4949, doi:10.1175/jcli-d-16-0180.1.
- 634 Graversen, R. G., and M. Wang, 2009: Polar amplification in a coupled climate model with
635 locked albedo, *Climate Dynam.*, **33**, 629-643, doi:10.1007/s00382-009-0535-6.
- 636 Graversen, R. G., T. Mauritsen, S. Drijfhout, M. Tjernström, and S. Mårtensson, 2011: Warm
637 winds from the Pacific caused extensive Arctic sea-ice melt in summer 2007, *Climate*
638 *Dynam.*, **36**, 2103-2112, doi:10.1007/s00382-010-0809-z.
- 639 Groves, D. G., and J. A. Francis, 2002: Variability of the Arctic atmospheric moisture budget
640 from TOVS satellite data, *J. Geophys. Res. Atmos.*, **107**, ACL 18-1-ACL 18-15,
641 doi:10.1029/2002JD002285.

- 642 Hanna, E., J. M. Jones, J. Cappelen, S. H. Mernild, L. Wood, K. Steffen, and P. Huybrechts, 2013:
643 The influence of North Atlantic atmospheric and oceanic forcing effects on 1900–2010
644 Greenland summer climate and ice melt/runoff, *Int. J. Climatol.*, **33**, 862–880,
645 doi:doi:10.1002/joc.3475.
- 646 Hewitson, B. C., and R. G. Crane, 2002: Self-organizing maps: applications to synoptic
647 climatology, *Clim. Res.*, **22**, 13–26.
- 648 Johansson, E., A. Devasthale, M. Tjernström, A. M. L. Ekman, and T. L'Ecuyer, 2017: Response of
649 the lower troposphere to moisture intrusions into the Arctic, *Geophys. Res. Lett.*, **44**,
650 2527–2536, doi:10.1002/2017GL072687.
- 651 Jun, S.-Y., C.-H. Ho, J.-H. Jeong, Y.-S. Choi, and B.-M. Kim, 2016: Recent changes in winter Arctic
652 clouds and their relationships with sea ice and atmospheric conditions, *Tellus A*, **68**,
653 29130, doi:10.3402/tellusa.v68.29130.
- 654 Koenigk, T., L. Brodeau, R. G. Graversen, J. Karlsson, G. Svensson, M. Tjernström, U. Willén, and
655 K. Wyser, 2013: Arctic climate change in 21st century CMIP5 simulations with EC-Earth,
656 *Climate Dynam.*, **40**, 2719–2743, doi:10.1007/s00382-012-1505-y.
- 657 Kohonen, T., 2001: Self-Organizing Maps. Springer-Verlag, 501 pp.
- 658 L'Heureux, M. L., A. Kumar, G. D. Bell, M. S. Halpert, and R. W. Higgins, 2008: Role of the Pacific-
659 North American (PNA) pattern in the 2007 Arctic sea ice decline, *Geophys. Res. Lett.*, **35**,
660 doi:10.1029/2008gl035205.
- 661 Liu, C., and E. A. Barnes, 2015: Extreme moisture transport into the Arctic linked to Rossby wave
662 breaking, *J. Geophys. Res. Atmos.*, doi:10.1002/2014JD022796.
- 663

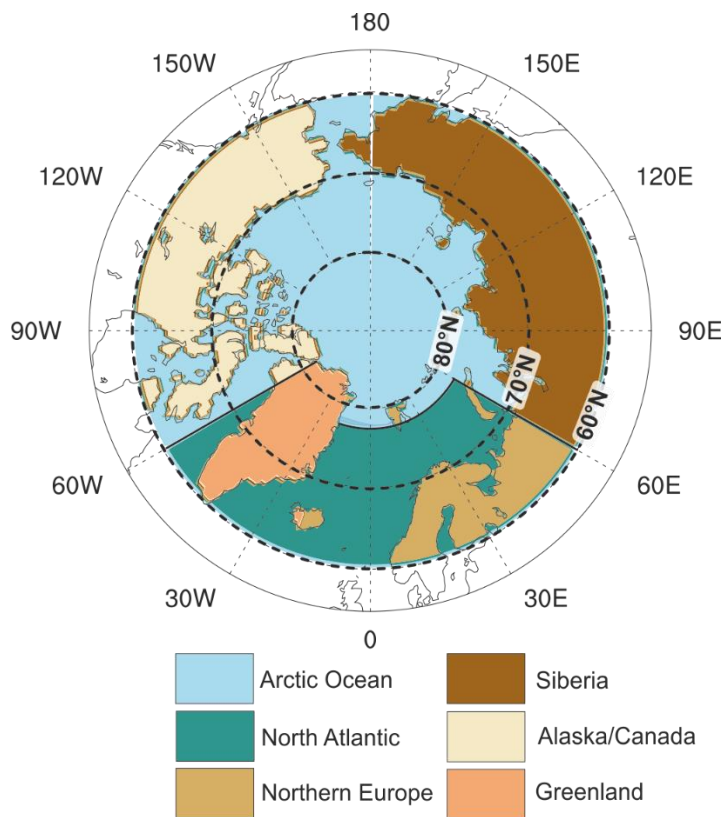
- 664 Liu, Y., and J. R. Key, 2016: Assessment of Arctic Cloud Cover Anomalies in Atmospheric
665 Reanalysis Products Using Satellite Data, *J. Clim.*, **29**, 6065-6083, doi:10.1175/jcli-d-15-
666 0861.1.
- 667 Liu, Y., J. R. Key, Z. Liu, X. Wang, and S. J. Vavrus, 2012: A cloudier Arctic expected with
668 diminishing sea ice, *Geophys. Res. Lett.*, **39**, doi:10.1029/2012GL051251.
- 669 Liu, Y., J. R. Key, S. Vavrus, and C. Woods, 2018: Time Evolution of the Cloud Response to
670 Moisture Intrusions into the Arctic during Winter, *J. Clim.*, **31**, 9389-9405,
671 doi:10.1175/jcli-d-17-0896.1.
- 672 Mattingly, K. S., C. A. Ramseyer, J. J. Rosen, T. L. Mote, and R. Muthyalu, 2016: Increasing water
673 vapor transport to the Greenland Ice Sheet revealed using self-organizing maps,
674 *Geophys. Res. Lett.*, **43**, 9250-9258, doi:doi:10.1002/2016GL070424.
- 675 Morrison, H., G. de Boer, G. Feingold, J. Harrington, M. D. Shupe, and K. Sulia, 2011: Resilience
676 of persistent Arctic mixed-phase clouds, *Nat. Geosci.*, **5**, 11, doi:10.1038/ngeo1332.
- 677 Morrison, A. L., J. E. Kay, W. R. Frey, H. Chepfer, and R. Guzman, 2019: Cloud Response to Arctic
678 Sea Ice Loss and Implications for Future Feedback in the CESM1 Climate Model, *J.*
679 *Geophys. Res. Atmos.*, **124**, 1003-1020, doi:10.1029/2018jd029142.
- 680 Naakka, T., T. Nygård, and T. Vihma, 2018: Arctic Humidity Inversions: Climatology and
681 Processes, *J. Clim.*, **31**, 3765-3787, doi:10.1175/jcli-d-17-0497.1.
- 682 Naakka, T., T. Nygård, T. Vihma, J. Sedlar, and R. G. Graversen, 2019: Atmospheric moisture
683 transport between mid-latitudes and the Arctic: regional, seasonal and vertical
684 distributions *Int. J. Climatol.* **1–18**, doi:10.1002/joc.5988.

- 685 Park, D.-S. R., S. Lee, and S. B. Feldstein, 2015: Attribution of the Recent Winter Sea Ice Decline
686 over the Atlantic Sector of the Arctic Ocean, *J. Clim.*, **28**, 4027-4033, doi:10.1175/jcli-d-
687 15-0042.1.
- 688 Pithan, F., and T. Mauritsen, 2014: Arctic amplification dominated by temperature feedbacks in
689 contemporary climate models, *Nature Geosci.*, **7**, 181-184, doi:10.1038/ngeo2071.
- 690 Pithan, F. and Coauthors, 2018: Role of air-mass transformations in exchange between the
691 Arctic and mid-latitudes, *Nat. Geosci.*, **11**, 805-812, doi:10.1038/s41561-018-0234-1.
- 692 Screen, J. A., and I. Simmonds, 2010: Increasing fall-winter energy loss from the Arctic Ocean
693 and its role in Arctic temperature amplification, *Geophys. Res. Lett.*, **37**,
694 doi:10.1029/2010GL044136.
- 695 Screen, J. A. and Coauthors, 2018: Consistency and discrepancy in the atmospheric response to
696 Arctic sea-ice loss across climate models, *Nat. Geosci.*, **11**, 155-163, doi:10.1038/s41561-
697 018-0059-y.
- 698 Shupe, M. D., and J. M. Intrieri, 2004: Cloud Radiative Forcing of the Arctic Surface: The
699 Influence of Cloud Properties, Surface Albedo, and Solar Zenith Angle, *J. Clim.*, **17**, 616-
700 628, doi:10.1175/1520-0442(2004)017<0616:crfota>2.0.co;2.
- 701 Shupe, M. D., 2011: Clouds at Arctic Atmospheric Observatories. Part II: Thermodynamic Phase
702 Characteristics, *J. Appl. Meteor. Climatol.*, **50**, 645-661, doi:10.1175/2010JAMC2468.1.
- 703 Skific, N., J. A. Francis, and J. J. Cassano, 2009: Attribution of Projected Changes in Atmospheric
704 Moisture Transport in the Arctic: A Self-Organizing Map Perspective, *J. Clim.*, **22**, 4135-
705 4153, doi:10.1175/2009JCLI2645.1.

- 706 Stroeve, J., and D. Notz, 2018: Changing state of Arctic sea ice across all seasons, *Environ. Res.*
707 *Lett.*, **13**, 103001.
- 708 Thompson, D. W. J., and J. M. Wallace, 1998: The Arctic oscillation signature in the wintertime
709 geopotential height and temperature fields, *Geophys. Res. Lett.*, **25**, 1297-1300,
710 doi:10.1029/98GL00950.
- 711 Tiedtke, M., 1993: Representation of Clouds in Large-Scale Models, *Mon. Weather Rev.*, **121**,
712 3040-3061, doi:10.1175/1520-0493(1993)121<3040:rocils>2.0.co;2.
- 713 Trenberth, K. E., 1991: Climate Diagnostics from Global Analyses: Conservation of Mass in
714 ECMWF Analyses, *J. Clim.*, **4**, 707-722, doi:10.1175/1520-
715 0442(1991)004<0707:cdfgac>2.0.co;2.
- 716 Vavrus, S. J., M. M. Holland, A. Jahn, D. A. Bailey, and B. A. Blazey, 2012: Twenty-First-Century
717 Arctic Climate Change in CCSM4, *J. Clim.*, **25**, 2696-2710, doi:10.1175/jcli-d-11-00220.1.
- 718 Vázquez, M., R. Nieto, A. Drumond, and L. Gimeno, 2016: Moisture transport into the Arctic:
719 Source-receptor relationships and the roles of atmospheric circulation and evaporation,
720 *J. Geophys. Res. Atmos.*, **121**, 13,493-13,509, doi:10.1002/2016JD025400.
- 721 Vihma, T. and Coauthors, 2016: The atmospheric role in the Arctic water cycle: A review on
722 processes, past and future changes, and their impacts, *J. Geophys. Res. Biogeosci.*, **121**,
723 586-620, doi:10.1002/2015JG003132.
- 724 Walsh, J. E., and W. L. Chapman, 1998: Arctic Cloud–Radiation–Temperature Associations in
725 Observational Data and Atmospheric Reanalyses, *J. Clim.*, **11**, 3030-3045,
726 doi:10.1175/1520-0442(1998)011<3030:acrtai>2.0.co;2.
- 727

- 728 Woods, C., R. Caballero, and G. Svensson, 2013: Large-scale circulation associated with
729 moisture intrusions into the Arctic during winter, *Geophys. Res. Lett.*, **40**, 4717-4721,
730 doi:10.1002/grl.50912.
- 731 Woods, C., and R. Caballero, 2016: The Role of Moist Intrusions in Winter Arctic Warming and
732 Sea Ice Decline, *J. Clim.*, **29**, 4473-4485, doi:10.1175/jcli-d-15-0773.1.
- 733 Zhong, L., L. Hua, and D. Luo, 2018: Local and External Moisture Sources for the Arctic Warming
734 over the Barents–Kara Seas, *J. Clim.*, **31**, 1963-1982, doi:10.1175/jcli-d-17-0203.1.

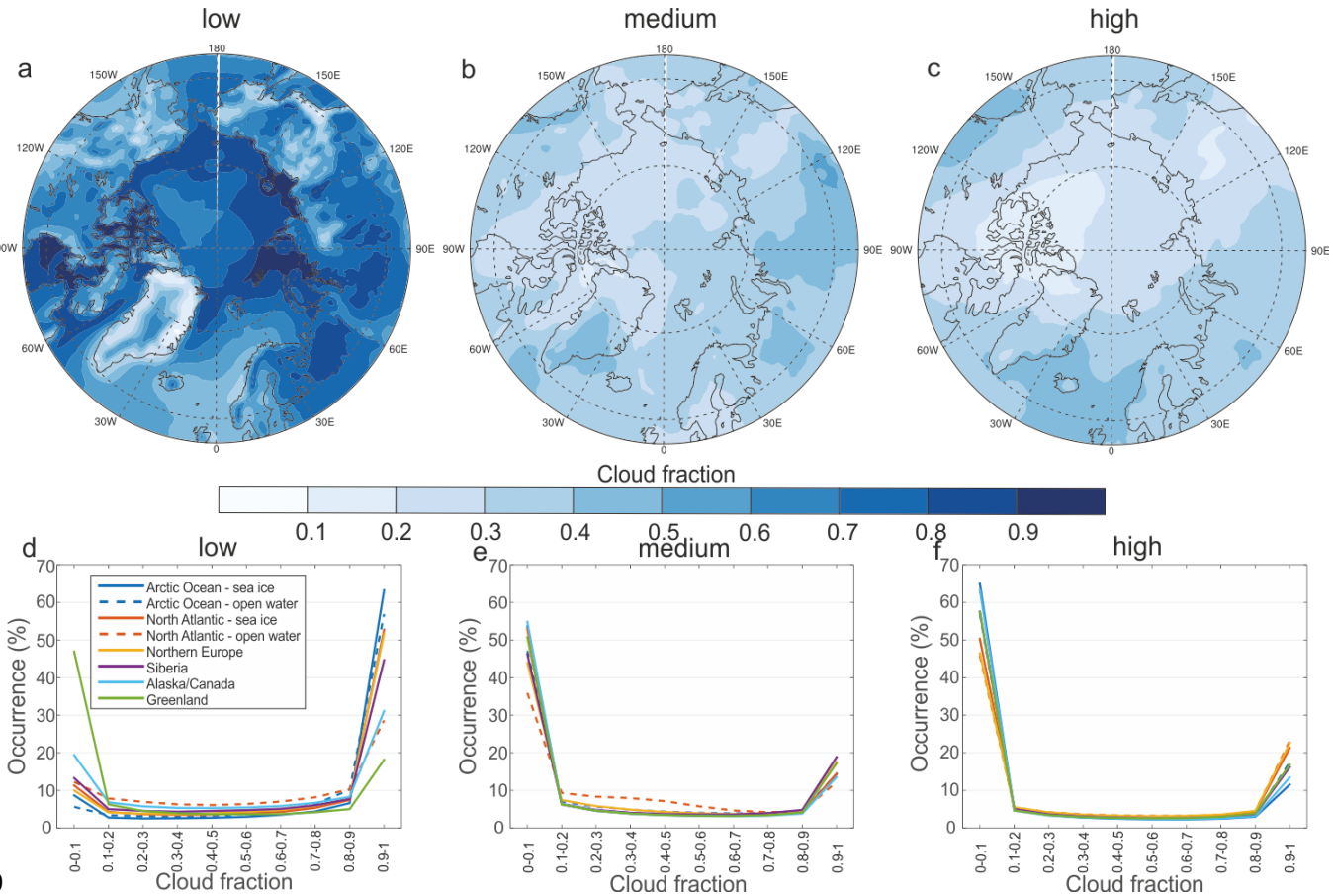
735



736

737

738 **Fig 1.** Map of sub-regions.



739

740

741 **Fig 2.** Winter (Dec-Feb) mean a) low cloud cover ($1.0 > \sigma > 0.8$), b) medium cloud cover ($0.8 > \sigma > 0.45$), and c) high cloud cover ($0.45 \geq \sigma$) in ERA-Interim (2003–2017). The sigma values in the brackets indicate the definitions of the clouds based on their altitudes, sigma being the pressure divided by the surface pressure. Regional cloud fraction occurrence distributions of

742 d) low clouds, e) medium clouds and f) high clouds. Definitions of the regions are shown in Fig.

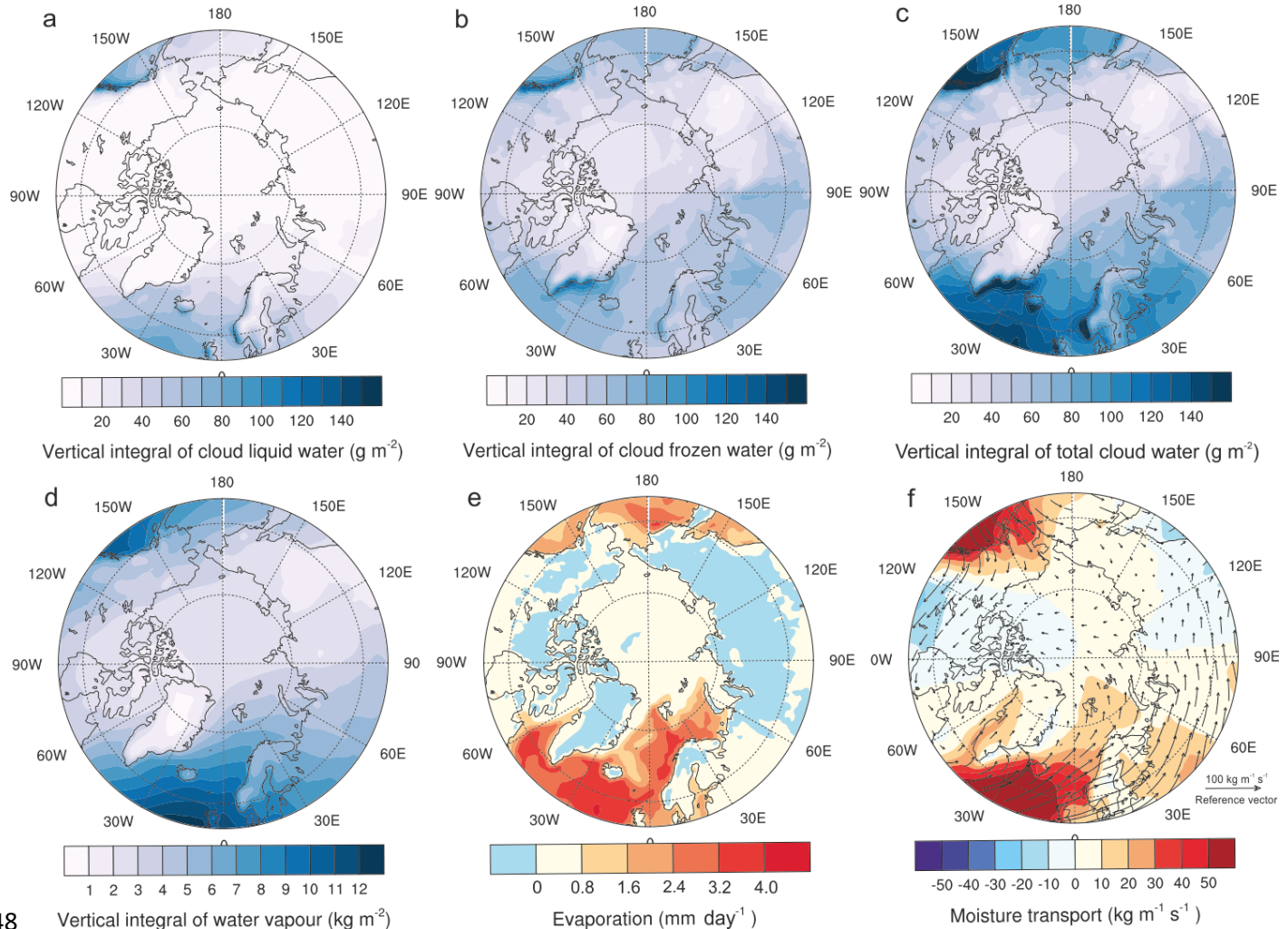
743

744

745

746 1.

747

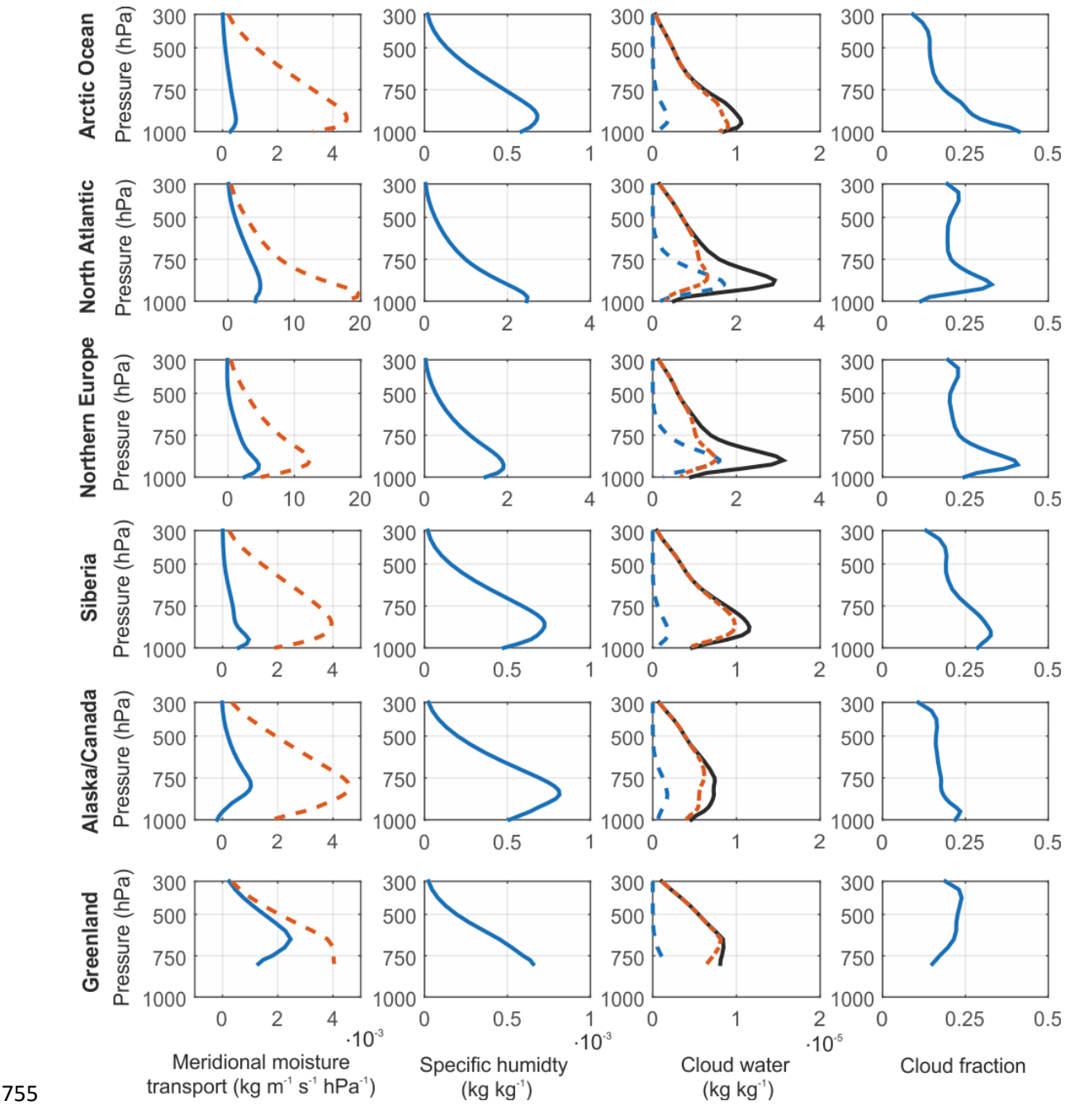


748 Vertical integral of water vapour (kg m^{-2})

749

750 **Fig 3.** Winter (Dec-Feb) mean a) vertically integrated cloud liquid water, b) vertically integrated
 751 cloud frozen water, c) vertically integrated total cloud water, d) vertically integrated water vapor,
 752 e) evaporation and f) net moisture transport in 2003–2017. In f), meridional net transport is
 753 indicated with colors, and the vectors denote the meridional and zonal net transport.

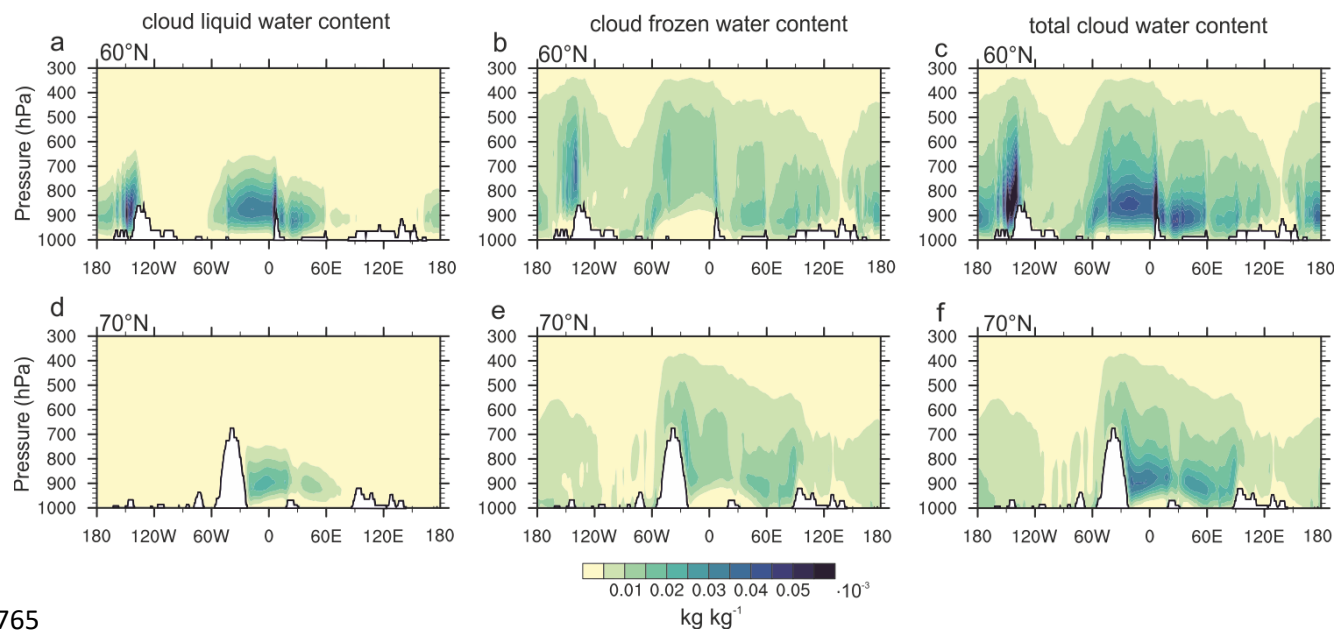
754



757 **Fig 4.** Vertical profiles of regionally averaged meridional moisture transport, specific humidity,
 758 cloud water and cloud fraction (in this order from the left) in winter (Dec-Feb). The blue solid line
 759 of meridional moisture transport shows the net meridional moisture transport and the red

760 dashed line shows the total meridional moisture transport (the sum of absolute northward and
761 southward transports). The total cloud water is shown with a black solid line, the frozen cloud
762 water with a red dashed line and liquid cloud water with a blue dashed line. Note that the scale
763 is different for the North Atlantic and Northern Europe relative to other regions.

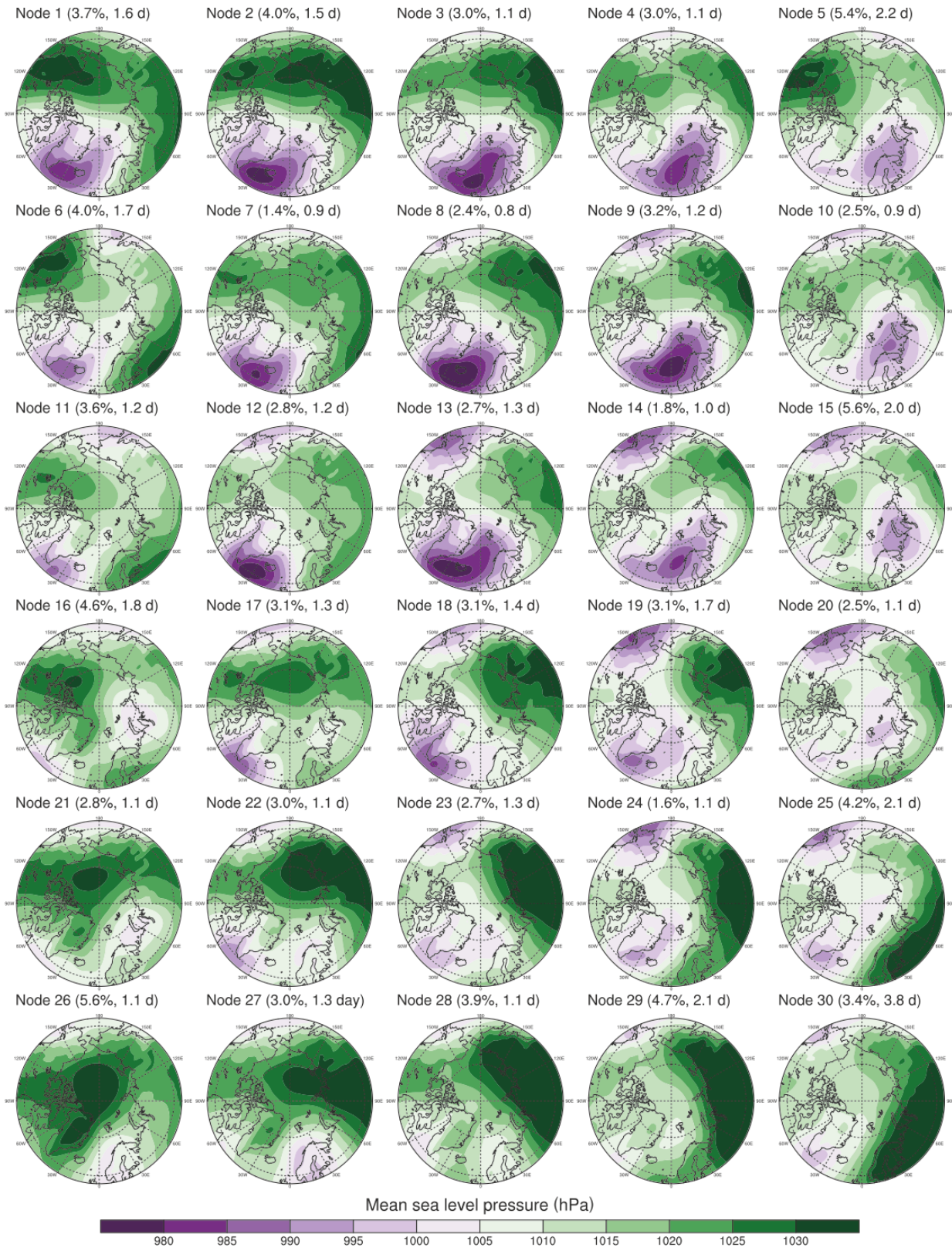
764



765

766 **Fig 5.** Cross section of a) and d) cloud liquid water content, b) and e) cloud frozen water
 767 content, and c) and f) total cloud water content on latitudes 60°N and 70°N in winter (Dec-Feb).

768

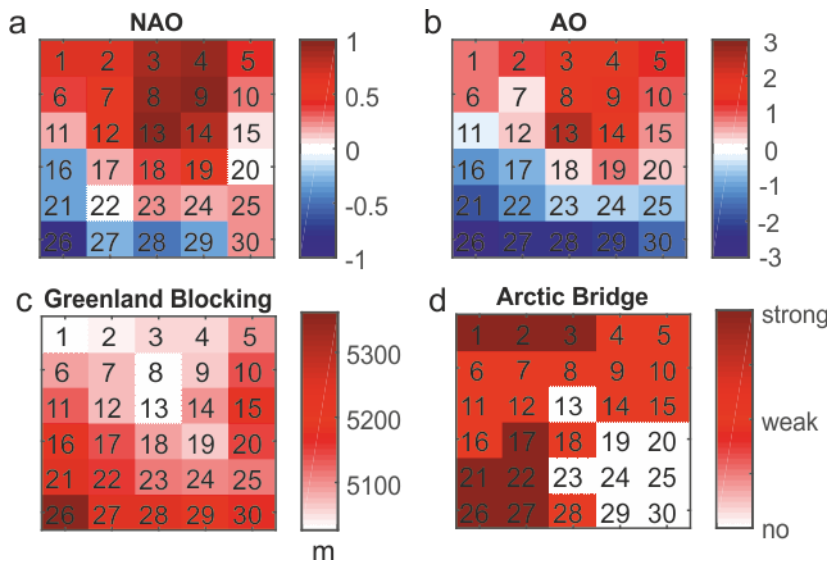


769

770 **Fig 6.** Mean sea level pressure averaged over the cases belonging to each of the SOM nodes in

771 winters (Dec-Feb) of 2003 – 2017. Relative frequency (of total 5416 cases) and mean

772 persistence of each node are shown in the brackets.

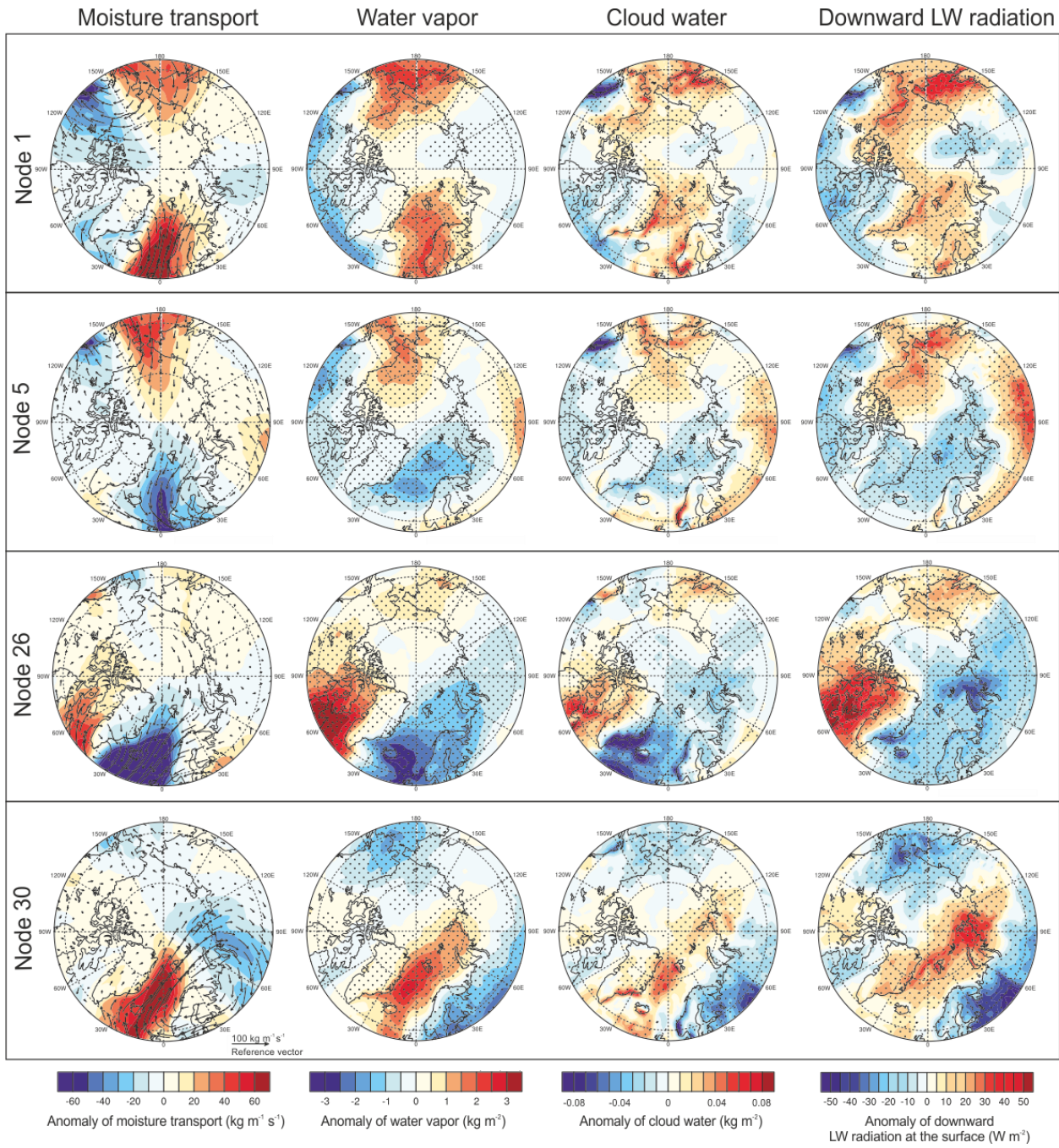


773

774

775 **Fig 7.** Mean values of a) the NAO, b) AO, and c) Greenland Blocking Index, and d) characterization
776 of the existence and strength of Arctic Bridge in the SOM nodes.

777



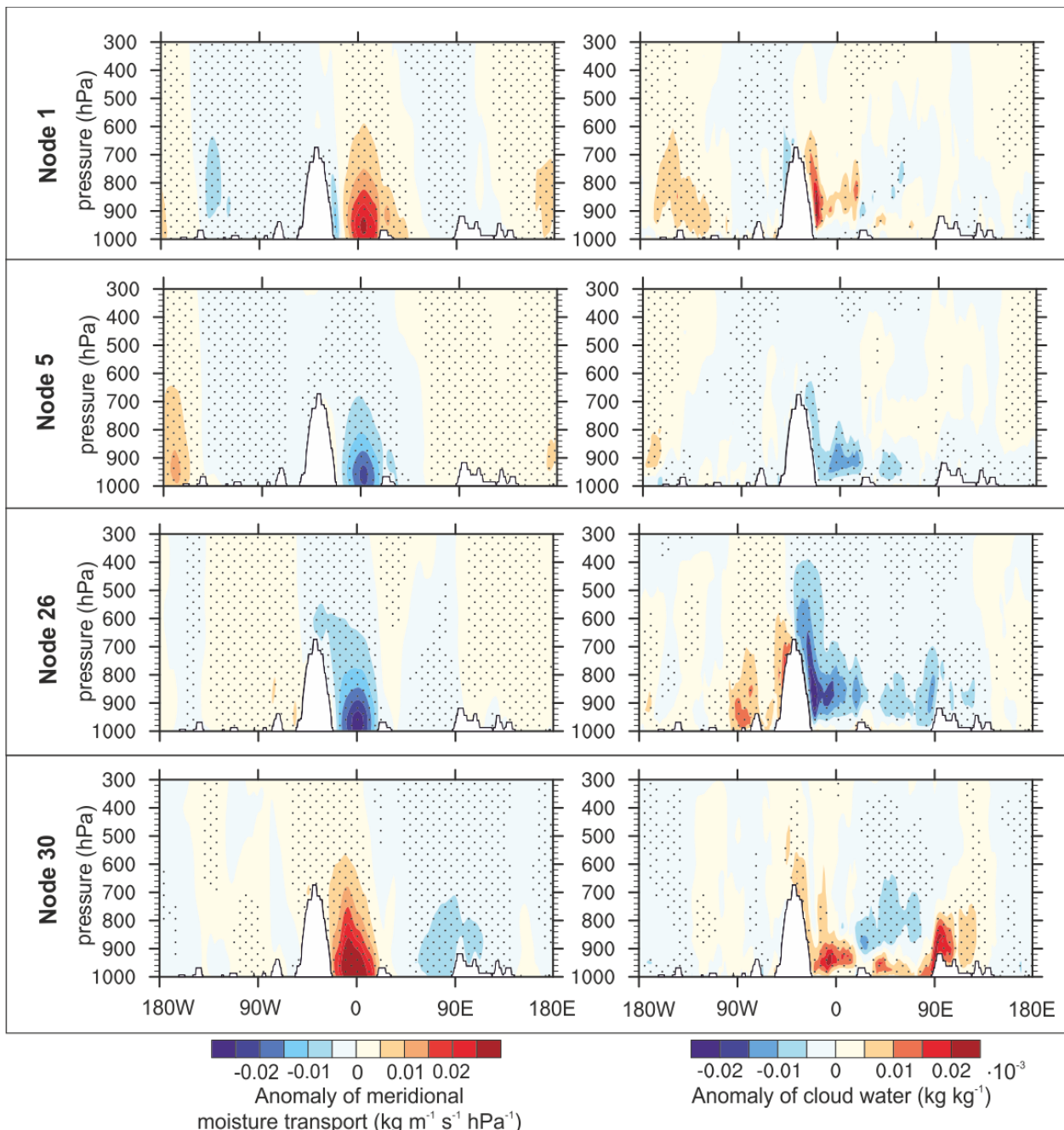
778

779 **Fig. 8** Anomalies of mean vertically integrated moisture transport (vectors show the anomaly of
 780 zonal and meridional transport whereas the colors show the anomaly of meridional transport
 781 only), vertically integrated water vapor, vertically integrated cloud water content and
 782 downward longwave radiation at the surface (in this order from the left to right) in four SOM

783 nodes. Dotted shadings show the anomalies that are different from zero at the 98% significance

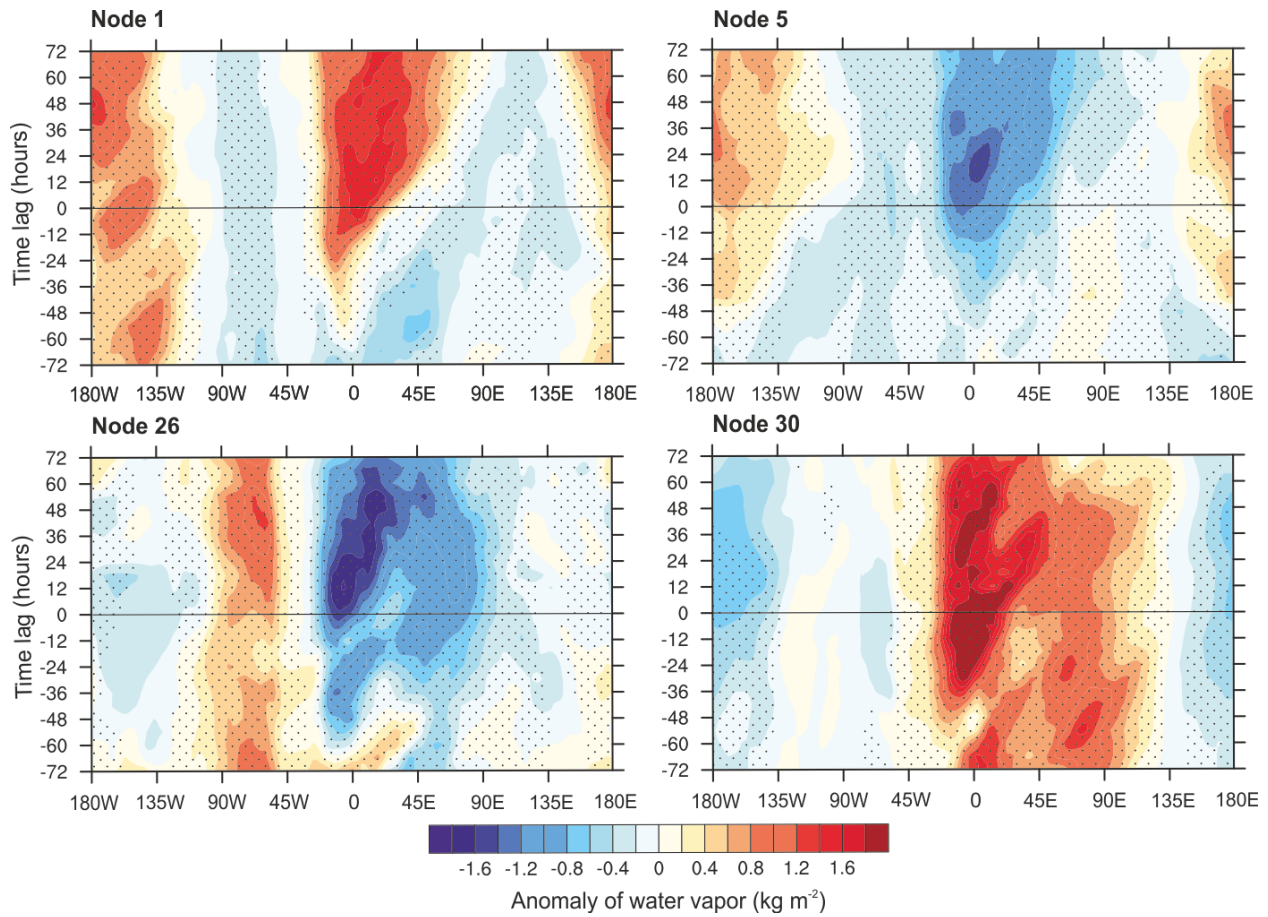
784 level (not shown for anomaly of moisture transport due to the vectors in the plot).

785



786

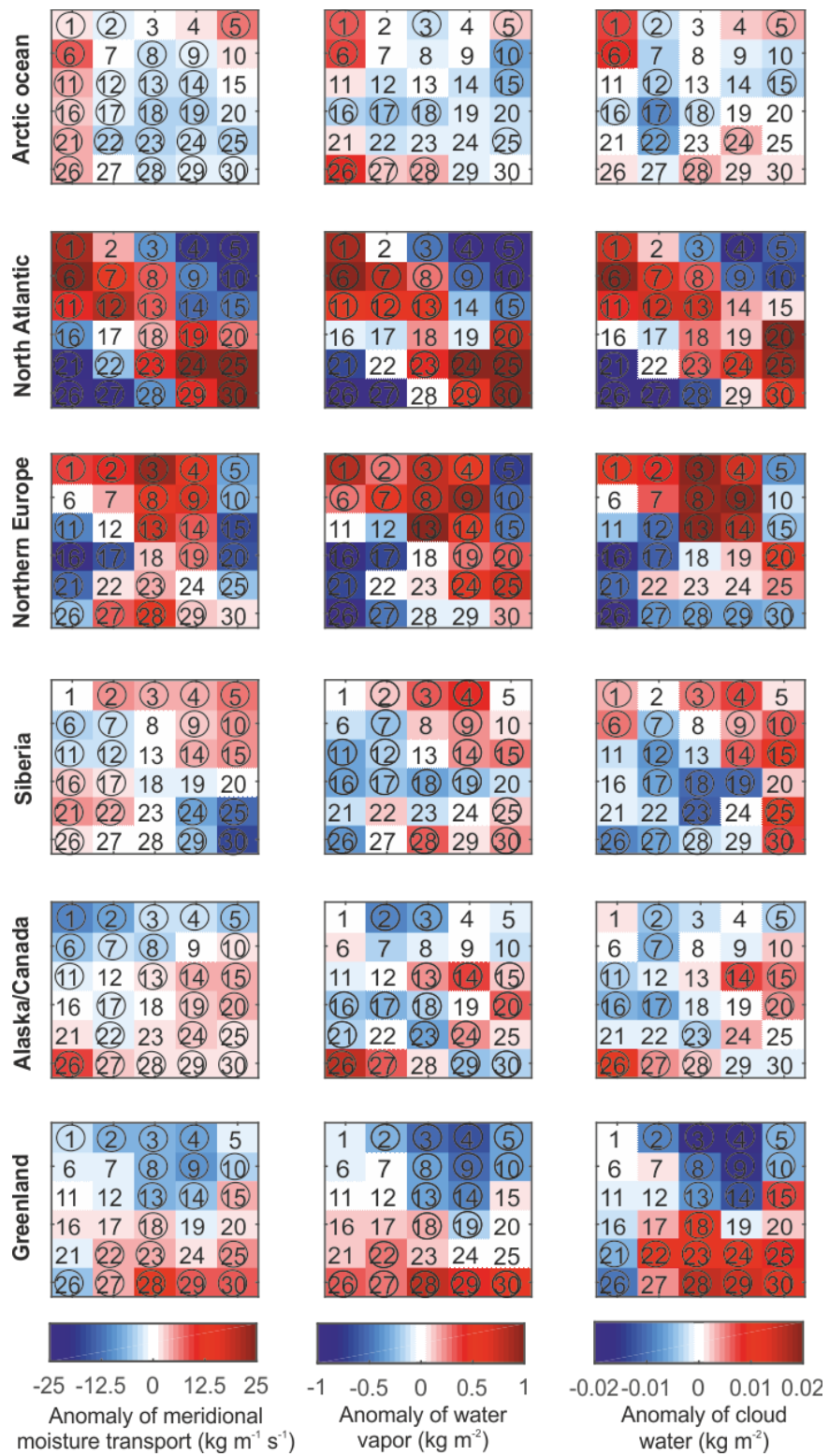
787 **Fig 9.** Anomalies of meridional moisture transport (left) and cloud water (right) at cross sections
 788 along 70°N in four SOM nodes. Dotted shadings show the anomalies that are different from zero
 789 at the 98% significance level.



790

791 **Fig 10.** Anomaly of vertically integrated water vapor, averaged between 70°N and 80°N , as a
 792 function of longitude and time lag in four SOM nodes. Positive values of time lag denote time
 793 elapsed since the start of a circulation regime (node). Dotted shadings show the anomalies that
 794 are different from zero at 98% significance level.

795



796

797 **Fig 11.** Regionally averaged anomalies of moisture transport (left), vertically integrated water
798 vapor (middle) and cloud water (right) in the different circulation regimes (SOM nodes marked

with 1–30). Anomalies that are different from zero at the 98% significance level are marked with circles.

801

802

803

804

805 **Supplemental Material**

806 **Uncertainties in the data**

807 To address the limited accuracy of ERA-Interim data, especially in the Arctic in winter, and its impacts on
808 the results of this study, we refer to previous studies.

809 Dufour et al. (2016) compared water vapour distributions and the meridional moisture flux of seven
810 reanalyses, including ERA-Interim, to radiosonde observations at the locations of Arctic radiosonde
811 stations in 1979–2017. They found that the specific humidity above the boundary layer was well captured
812 by the reanalyses, and the vertically integrated water vapour was slightly lower in the reanalyses than in
813 the observations. In addition, the meridional moisture flux of reanalyses was qualitatively in agreement
814 with observations in terms of longitudinal, vertical and temporal patterns, although the flux was 10%
815 higher in ERA-Interim than in the radiosonde observations. Importantly, ERA-Interim captured the altitude
816 of the maximum net moisture transport flux located at 850 hPa.

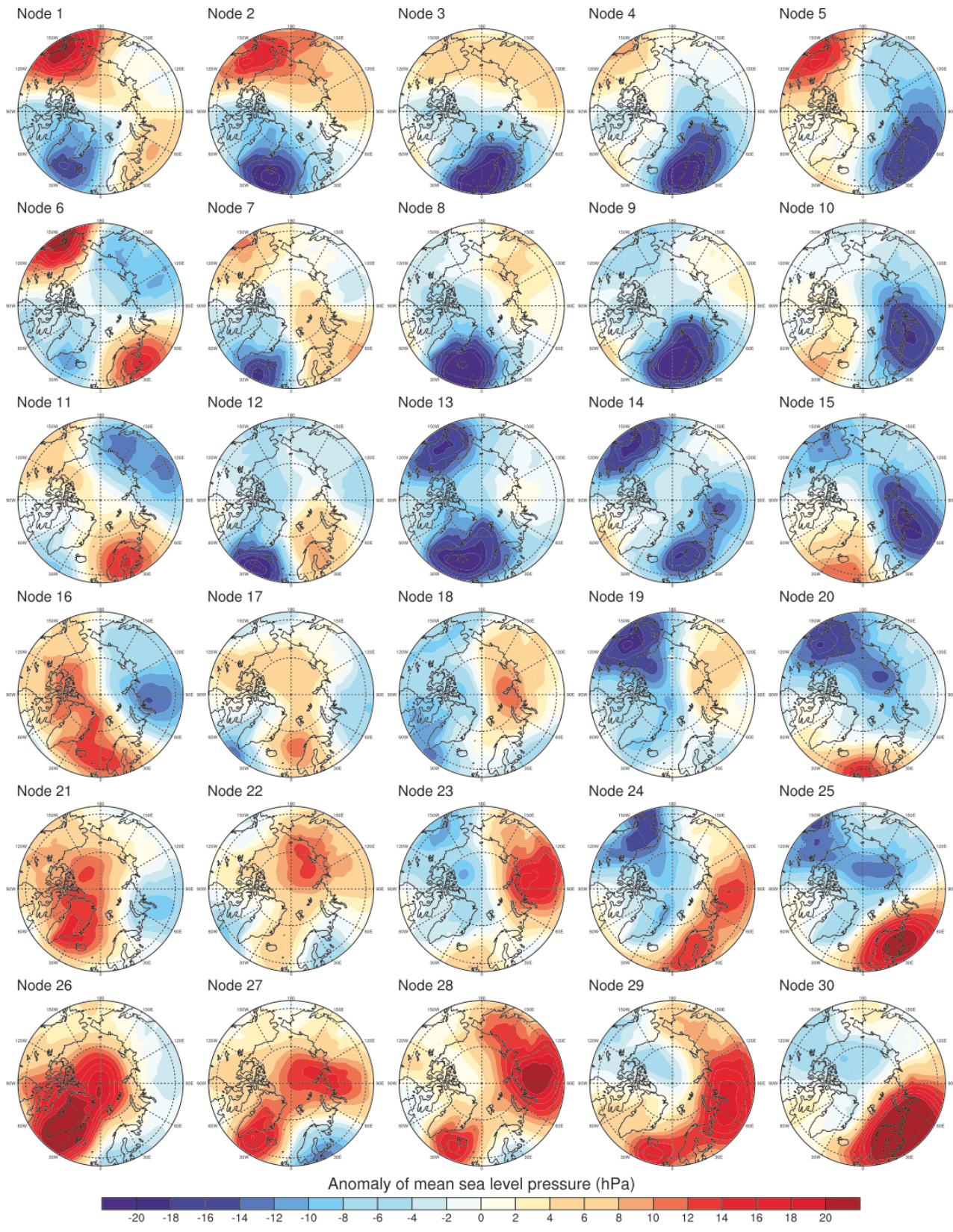
817 The skill of ECMWF cloudiness forecasts is improved if time-averages are used instead of the
818 instantaneous values (Haiden et al. 2015). Liu and Key (2016) reported differences in the mean cloud
819 amount in reanalyses compared to satellite observations by Moderate Resolution Imaging
820 Spectroradiometer (MODIS) and Cloud–Aerosol Lidar and Infrared Pathfinder Satellite Observation
821 (CALIPSO), but concluded that reanalyses (including ERA-Interim) have better capability for depicting the
822 monthly cloud amount anomalies than the mean cloud amount in the Arctic. In their study, ERA-Interim
823 showed a higher cloud amount in winter compared to MODIS and CALIPSO. It is, however, important to
824 note that also satellite observations have large errors in wintertime; passive satellite instruments suffer
825 from the absence of shortwave radiation and existence of temperature inversions, whereas active sensors
826 have difficulties to detect low clouds (Zygmuntowska et al. 2012). Liu and Key (2016) also reported that
827 the reanalyses perform better for cloud amount anomalies over land than over the ocean, and suggested
828 that this is due to more observations assimilated over land areas than over sea.

829 According to Sotiropoulou et al. (2014), the lack of liquid layers in clouds at temperatures lower than -
830 23°C, and thereby the inability of the cloud scheme to represent common mixed-phase clouds in a
831 physically correct way, are critical deficiencies in the cloud scheme of ERA Interim. However, Cox et al.
832 (2014) found that ERA-Interim performed reasonably well in depicting downward longwave radiation at
833 Summit in Greenland, although ERA-Interim presumably included too many thin clouds and too few thick
834 clouds. They proposed that the errors were presumably more related to cloud generation processes than
835 persistent errors in the spatial positioning of air masses. In an evaluation of seven reanalyses in the Arctic,
836 ERA-Interim was found to have the smallest bias in downward longwave radiation (Lindsay et al. 2014).

837 In summary, ERA-Interim is a state-of-the-art data set and its accuracy can be considered as sufficient
838 when it comes to an investigation of relationships between atmospheric large-scale circulation, and
839 moisture and cloud distributions. The main focus of this study is on anomalies. Anomalies of clouds are
840 considered as more trustworthy than mean values (Liu and Key 2016), although anomalies are also liable
841 to notable uncertainties in their response to large-scale circulation, due to possible misrepresentation of
842 physical processes related to clouds and turbulence in the reanalysis. We presume that the largest
843 uncertainties in this study are related to cloud phases, and we are therefore careful for not drawing too
844 far conclusions based on the cloud phase. We also acknowledge that the higher cloud amount of ERA-

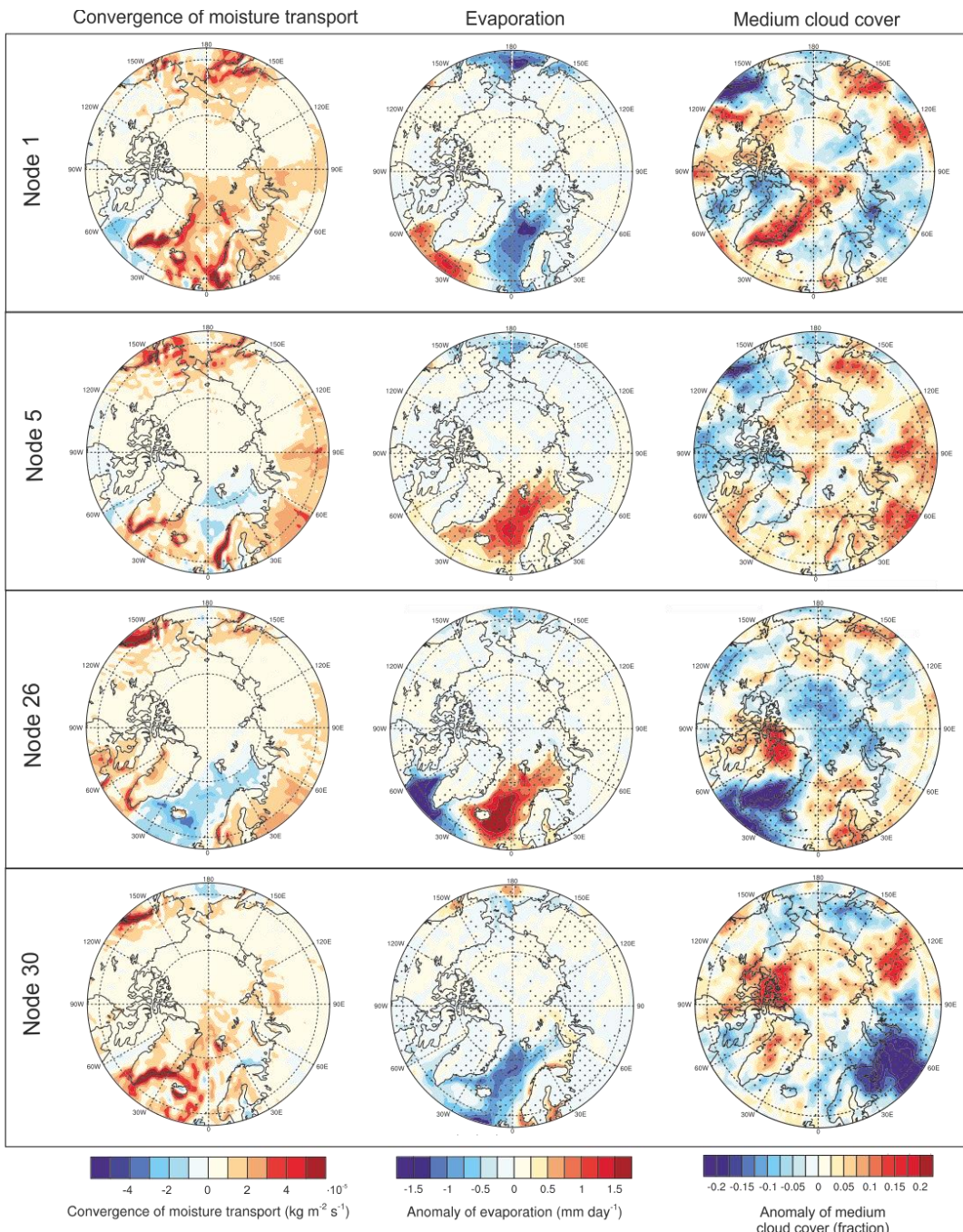
845 Interim compared to satellite observations and the challenges to represent mixed-phase clouds in low
846 temperatures probably have impacts on the accuracy of downward longwave radiation in ERA-Interim.

847



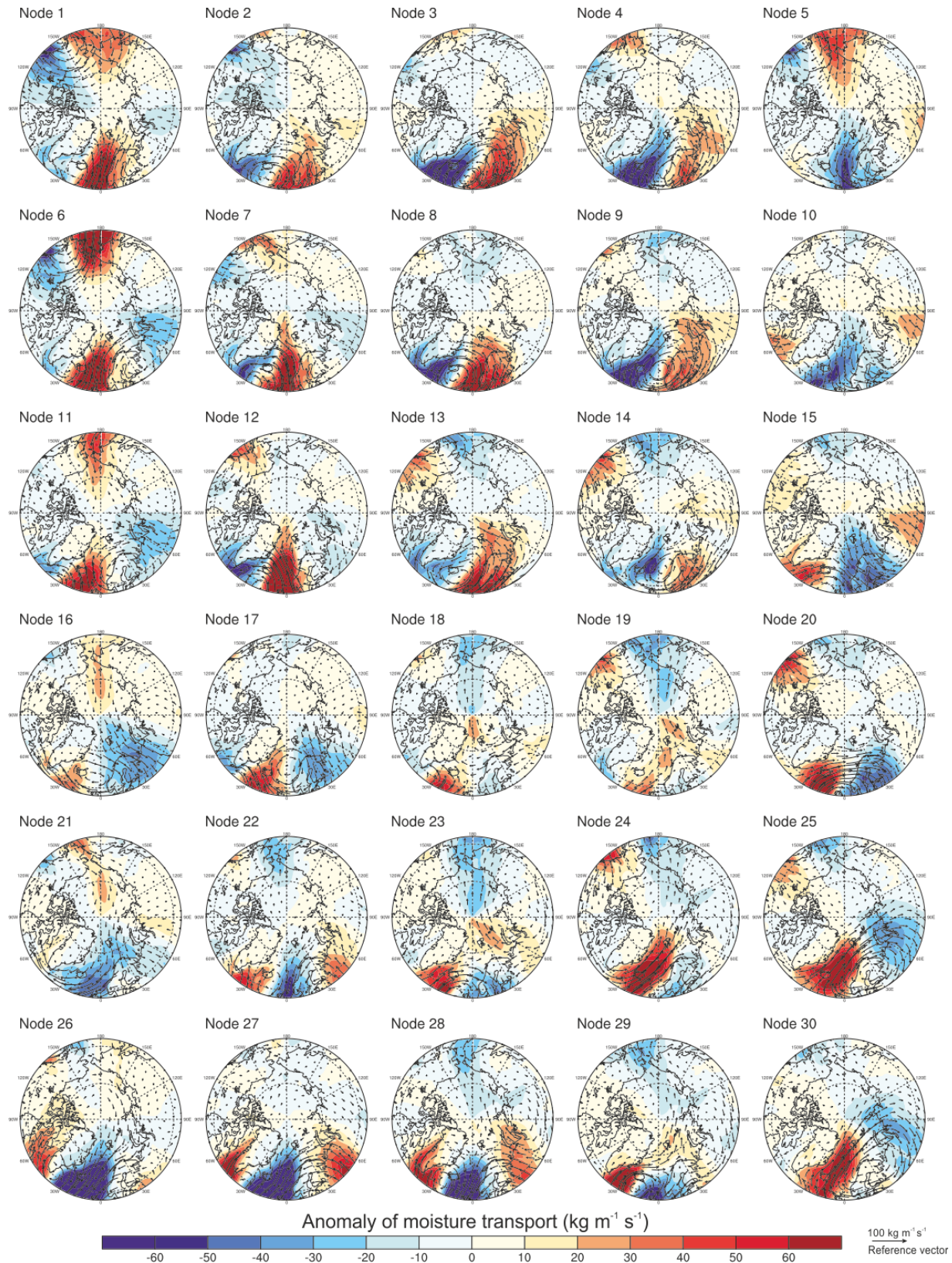
848

849 **Fig S1.** Anomaly of mean sea level pressure averaged over the cases belonging to each of the SOM
 850 nodes in winters (Dec-Feb) of 2003 – 2017.

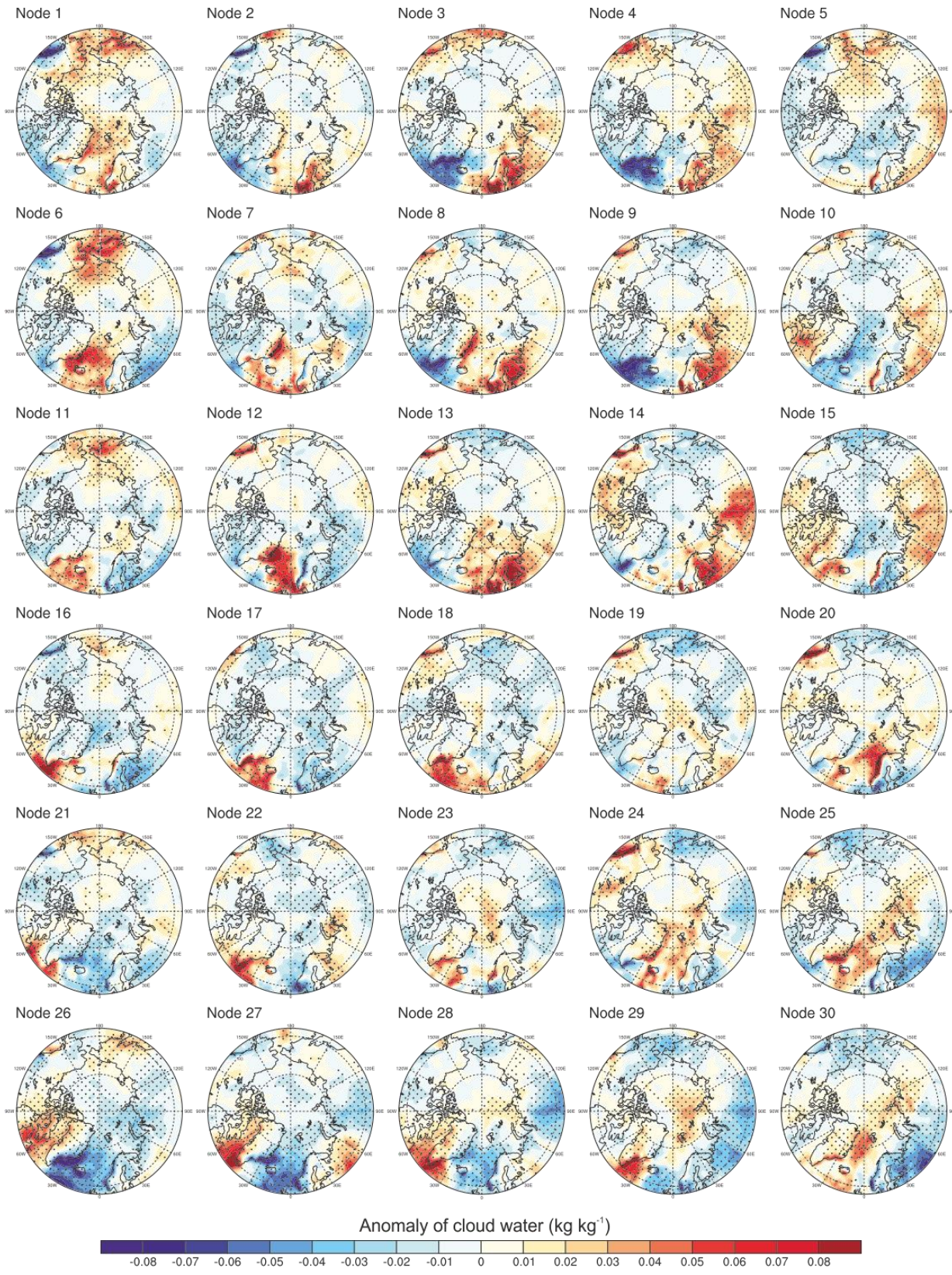


851

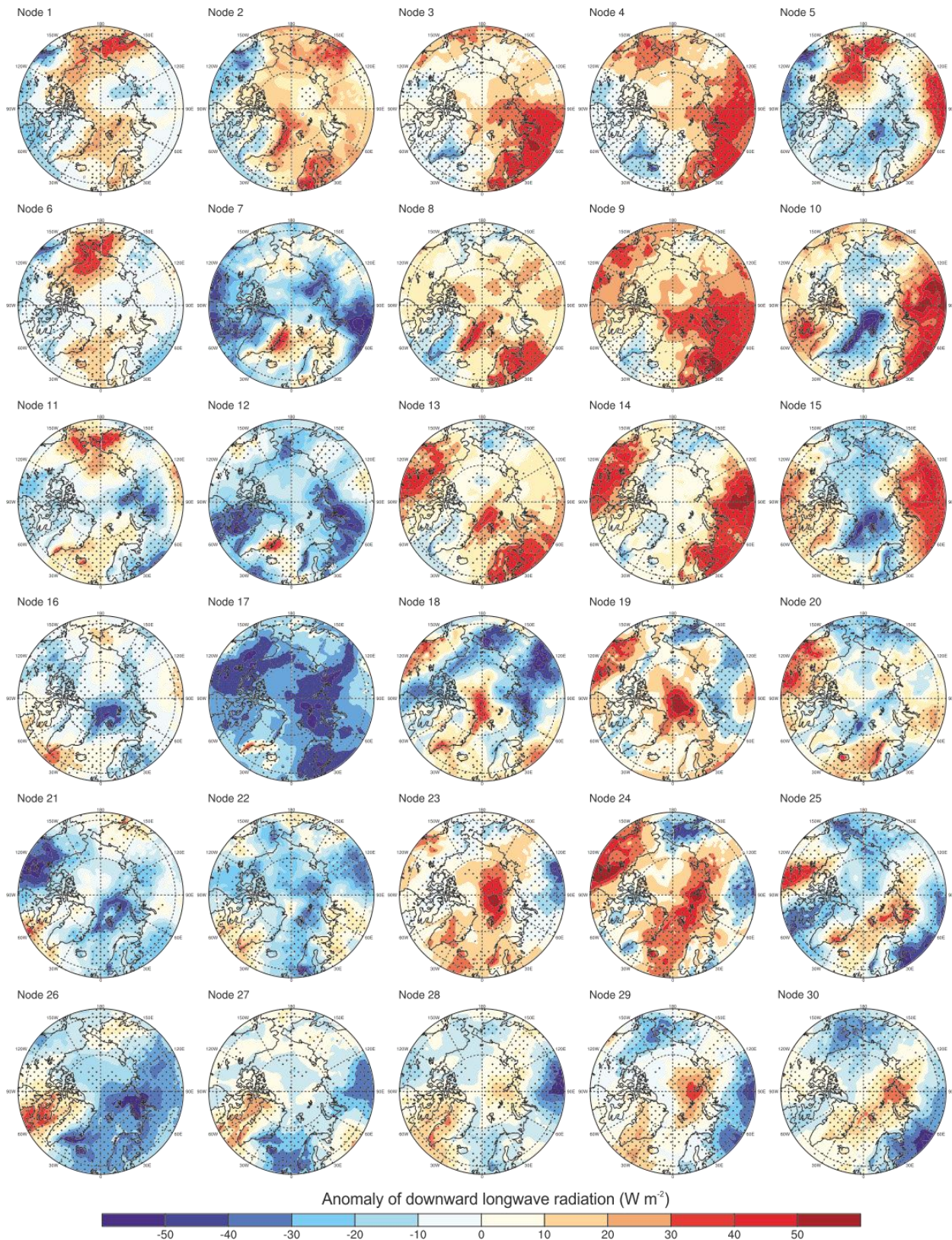
852 **Fig S2.** Convergence of horizontal moisture transport (left) and anomaly of evaporation (middle), and
 853 anomaly of medium cloud cover in four SOM nodes. Dotted shadings show the anomalies that are
 854 significantly different from zero at the 98% level.



856 **Fig S3.** Anomaly of horizontal moisture transport averaged over the cases belonging to each of the SOM
857 nodes in winters (Dec-Feb) of 2003 – 2017. Vectors show the anomaly of zonal and meridional transport
858 whereas the colors show the anomaly of meridional transport only.



860 **Fig S4.** Anomaly of cloud water averaged over the cases belonging to each of the SOM nodes in winters
861 (Dec-Feb) of 2003 – 2017. Dotted shadings show the anomalies that are significantly different from zero
862 at 98% level.



864 **Fig S5.** Anomaly of downward longwave radiation at the surface averaged over the cases belonging to
865 each of the SOM nodes in winters (Dec-Feb) of 2003 – 2017. Dotted shadings show the anomalies that
866 are significantly different from zero at 98% level.

867

868 **References**

- 869 Cox, C. J., V. P. Walden, G. P. Compo, P. M. Rowe, M. D. Shupe, and K. Steffen, 2014: Downwelling
870 longwave flux over Summit, Greenland, 2010–2012: Analysis of surface-based observations and
871 evaluation of ERA-Interim using wavelets, *J. Geophys. Res. Atmos.*, **119**, 12,317-12,337,
872 doi:10.1002/2014JD021975.
- 873 Dufour, A., O. Zolina, and S. K. Gulev, 2016: Atmospheric Moisture Transport to the Arctic: Assessment
874 of Reanalyses and Analysis of Transport Components, *J. Clim.*, **29**, 5061-5081, doi:10.1175/JCLI-
875 D-15-0559.1.
- 876 Haiden, T., R. M. Forbes, M. Ahlgrimm, and A. Bozzo: The skill of ECMWF cloudiness forecasts, ECMWF
877 Newsletter, pp. 14-19, 2015.
- 878 Lindsay, R., M. Wensnahan, A. Schweiger, and J. Zhang, 2014: Evaluation of Seven Different Atmospheric
879 Reanalysis Products in the Arctic, *J. Clim.*, **27**, 2588-2606, doi:10.1175/jcli-d-13-00014.1.
- 880 Liu, Y., and J. R. Key, 2016: Assessment of Arctic Cloud Cover Anomalies in Atmospheric Reanalysis
881 Products Using Satellite Data, *J. Clim.*, **29**, 6065-6083, doi:10.1175/jcli-d-15-0861.1.
- 882 Sotiropoulou, G., J. Sedlar, M. Tjernström, M. D. Shupe, I. M. Brooks, and P. O. G. Persson, 2014: The
883 thermodynamic structure of summer Arctic stratocumulus and the dynamic coupling to the
884 surface, *Atmos. Chem. Phys.*, **14**, 12573-12592, doi:10.5194/acp-14-12573-2014.
- 885 Zygmuntowska, M., T. Mauritsen, J. Quaas, and L. Kaleschke, 2012: Arctic Clouds and Surface Radiation –
886 a critical comparison of satellite retrievals and the ERA-Interim reanalysis, *Atmos. Chem. Phys.*,
887 **12**, 6667-6677, doi:10.5194/acp-12-6667-2012.

888

889

890

891